July 2017

Customizing Vehicular Ad Hoc Networks to Individual Drivers and Traffic Conditions

Ali Rakhshan

CUSTOMIZING VEHICULAR AD HOC NETWORKS TO INDIVIDUAL DRIVERS AND TRAFFIC CONDITIONS

A Dissertation Presented

by

ALI RAKHSHAN

Submitted to the Graduate School of the
University of Massachusetts Amherst in partial fulfillment
of the requirements for the degree of

DOCTOR OF PHILOSOPHY

May 2017

Electrical and Computer Engineering

CUSTOMIZING VEHICULAR AD HOC NETWORKS TO INDIVIDUAL DRIVERS AND TRAFFIC CONDITIONS

A Dissertation Presented

by

ALI RAKHSHAN

Approved as to style and content by:

H. Pishro-Nik, Chair

D. L. Goeckel, Member

M. F. Duarte, Member

Daiheng Ni, Member

Christopher Hollot, Department Chair
Electrical and Computer Engineering

To my parents.

ACKNOWLEDGMENTS

I would like to thank many professors at UMass, especially Prof. Hossein Pishro-Nik (my Ph.D. advisor), Prof. Dennis Goeckel, Prof. Marco Duarte, Prof. Daiheng Ni, Prof. Patrick Kelly, Prof. Christopher Hollot, Prof. Donald Fisher, and Prof. Amir Houmansadr. In addition, I would like to thank my former colleagues Dr. Mohammad Nekoui and Dr. Evan Ray. During my time at UMass Amherst, I was lucky to have wonderful labmates and to meet many amazing people.

ABSTRACT

CUSTOMIZING VEHICULAR AD HOC NETWORKS TO INDIVIDUAL DRIVERS AND TRAFFIC CONDITIONS

MAY 2017

ALI RAKHSHAN

M.Sc., UNIVERSITY OF MASSACHUSETTS AMHERST

Ph.D., UNIVERSITY OF MASSACHUSETTS AMHERST

Directed by: Professor H. Pishro-Nik

This dissertation studies the ability to individualize vehicular ad hoc networks (VANETs) in order to improve safety. Adapting a VANET to both its individual drivers' characteristics and traffic conditions enables it to transmit in a smart manner to other vehicles. This improvement is now possible due to the progress that is being made in VANETs.

To accomplish this adaptation, our approach is to use VANET data to learn drivers' characteristics. This information along with the traffic data, can be used to customize the VANETs to individual drivers. In this dissertation, we show that this process benefits all the drivers by reducing the collision probability of the network of vehicles. Our Monte Carlo simulation results show that this approach achieves more than 25% reduction in traffic collision probability compared to the case with optimized equal vehicular communication access for each vehicle. Therefore, it has a considerable advantage over other systems.

First, we propose a method to estimate the distribution of a driver's characteristics by employing the VANET data. This is essential for our intended application in accident warning systems and vehicular communications.

Second, this estimated distribution and the traffic information are used to adapt the transmission rates of vehicles to each driver's safety level in order to reduce the number of collisions in the network. We derive the packet success probability for a chain of vehicles by taking multi-user interference, path loss, and fading into account. Then, by considering the delay constraints and types of potential collisions, we approximate the required channel access probabilities and illustrate the collision probability.

Third, since the packet success probability and thus communication interference affect the collision probability noticeably, we examine various interference models and their effect on the collision probability with more scrutiny. In our analysis, two signal propagation models with and without carrier sensing are considered for the dissemination of periodic safety messages, and it is illustrated how employing more accurate interference models results in a higher level of safety (lower collision probability)for the network.

Finally, there is an unclear relation between the intensity of an ad hoc network (the number of vehicles in a certain area) and the performance of the system. Hence, we study a reverse approach in which the geometry (intensity) of the unmanned aerial vehicles varies and certain requirements such as safety and coverage need to be satisfied. The numerical results show that safety and interference limits the coverage of the network and there is only a relatively small range of intensities which satisfy all three.

TABLE OF CONTENTS

LIST OF TABLES

Table **Page**

LIST OF FIGURES

Figure **Page**

INTRODUCTION

During the past decade, the automobile industry has seen a surge in the use of advanced technologies, such as state-of-the-art electronic devices, in order to improve automobile safety. However, the fatalities and injuries caused by automobile accidents have remained at alarming levels. In particular, statistics from 2013 [1] report over five million crashes in the U.S., causing over two million injuries and more than 30,000 fatalities.

To best explain our idea of this dissertation, let us consider a safety application of a simple VANET. Fig. 1 depicts a scenario in which a chain of vehicles are following another vehicle (V0) on a highway when the lead vehicle (V0) suddenly begins to decelerate to avoid an unexpected obstacle, or due to a mechanical failure. Then, the following vehicle (V1) must also brake to avoid a collision. However, the driver of the following vehicle (V1) will take a certain amount of time to first perceive that he or she must brake (perception time), and then another length of time to actually apply the brake (reaction time).

Perception reaction time (PRT) [1] has undergone much scrutiny within the human factors literature. This time could increase as a result of various factors such as whether the driver is distracted or expecting a hazard. If the driver does not have sufficient time to react, a collision could occur, resulting in damage to the vehicles, or even injury or loss of life for the drivers or any passengers. Thus, any system that could help the driver of the following vehicle to react more quickly would be greatly

[1] Hereafter, we use perception reaction time (PRT) and brake response time (BRT) interchangeably, but in general, BRTs are just a special case of PRTs.

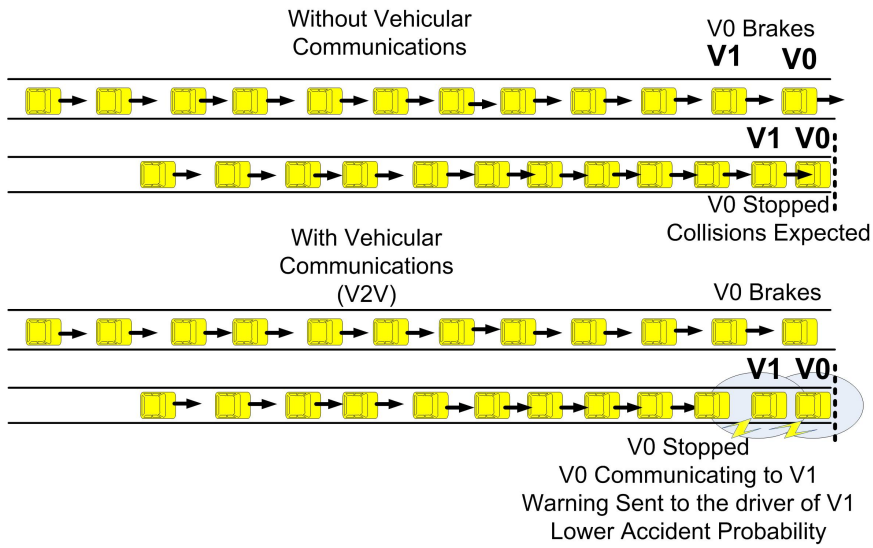

Figure 1: An example on how communications between vehicles can avoid a collision

beneficial. One such system is a simple warning. This could consist of both visual and auditory cues such as a warning light flashing, and an alarm being sounded. After receiving the warning, the driver could react more quickly, since the driver would understand that the warning indicates that he or she must brake immediately, and no thought will be required to assess the situation and decide on the best course of action. Such a system must be used carefully. With time, drivers may come to trust and rely on the warning system. Then, the system failing to provide a warning when one is needed could prove disastrous, as the driver may not react in time and collide with the leading vehicle. On the other hand, if the warnings that are given turn out to be false alarms too frequently, drivers may begin to ignore them. This would negate any safety benefit of the system, and could even reduce overall safety if the warnings become a distraction. This means that the system must attempt to minimize the frequency of false alarms while still maintaining a high level of safety.

Current efforts in the realm of intelligent transportation systems (ITS) typically consider drivers that can show a wide variety of behaviors during a driving session. Yet we all know that a specific driver has specific driving behaviors. He or she could

be vigilant or distracted; could perceive and react soon to an event or might have a longer PRT; could be aggressive in acceleration/deceleration or could be smoother in those. Since existing collision warning algorithms do not use the PRT distribution of individuals, drivers with different PRT in the same scenario receive the same warnings. Clearly, this approach is not the best for the design of safety systems.

A major cause of accidents is the slow response time of drivers to stopped traffic, i.e., the average time a driver takes to hit the brake after a preceding car has stopped. The cumulative response times for the leading vehicles are the critical element in the collision probability [2] of the upstream vehicles, potentially resulting in domino-style collisions. To reduce the drivers' response time to accidents, recent research and development in the automobile industry has introduced collision warning systems to be installed on modern automobiles. Collision warning systems are capable of cautioning about critical, time-sensitive incidents such as crashes or traffic jams.

With the advancements in VANETs (Fig. 2), recent research [2] suggests the use of VANETs to improve the effectiveness of collision warning systems. VANETs allow for cross-communication between cars within a close proximity of each other, which can enable them to efficiently and reliably communicate sensitive traffic messages such as crash-relevant information.

The Federal Communications Commission has allocated 75 MHz of spectrum in the 5.9 GHz band for Dedicated Short Range Communications (DSRC). To serve as the groundwork for DSRC, the IEEE 802.11p standard was published in the year 2010 for Wireless Access in Vehicular Environments (WAVE) [3]. Each vehicle in Fig. 2 is equipped with a wireless on-board equipment (OBE) which most importantly includes a CPU, a transceiver, and a GPS receiver. Using DSRC antennas, these vehicles are able to communicate with each other as well as with roadside equipment

[2]Hereafter, the term collision shall refer to vehicle collisions unless explicitly stated to denote packet collisions.

Figure 2: VANET: Vehicular Ad-hoc NETwork

(RSE). The transmitted data will be used in many applications such as providing the traffic management centers with accurate data on local traffic to make them capable of improving the mobility of the travelling vehicles. This data is more reliable than what low-cost Global Positioning System (GPS) devices can estimate.

The 75 MHz spectrum of DSRC is divided into seven 10 MHz-wide channels. One channel is called the control channel (CCH) and is used exclusively for safety messages. The other channels are called service channels (SCH) and are reserved for commercial applications. Safety messages are either event-driven or periodic. Each vehicle sends periodic messages in a single hop regularly in order to inform other vehicles inside its given neighborhood of important information such as location, speed, and acceleration while it sends event-driven messages to warn other vehicles of a collision.

In order to improve drivers' safety using the personalized vehicular communications, first we need to know the delay requirements of the safety applications. In general, the difference between the communication delay and the sum of PRTs of drivers

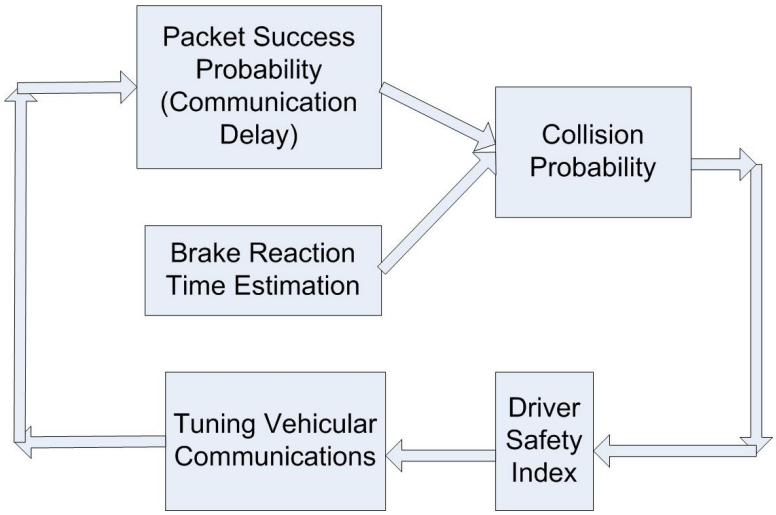

Figure 3: Optimizing loop of VANET for Collision Warning Systems

in a chain is the most important factor in reducing the average collision probability of the vehicles. Next, we need to know about the uncertainty of the packet delivery between two specific vehicles while other vehicles might also transmit simultaneously, thus interfering with the selected packet transmission. Deriving the probability of successful packet delivery helps us with finding the communication delay to inform each vehicle in a chain while employing vehicular communications. It is desirable to reduce this delay as much as possible by lessening the interference caused by other vehicles. Our proposed algorithm tunes this transmission probability of each vehicle based on the individual characteristics of drivers and the traffic conditions around the vehicles.

We also show that a safety index is needed for each driver and it must depend on the collision probability of the vehicle. This index can be learned by the system in real time as a function of the factors such as speed, acceleration, lane position and distance from the neighbors to customize the communication. Vehicle sensors (such as radars and cameras), installed on the vehicles, obtain this information. Radar sensors employ radio waves to detect objects (vehicles and pedestrians) and to find their position and velocity while cameras are usually combined with radars to provide a

more accurate and reliable detection. We need to make it clear that we do not expect to have access to information about the age of a driver, or any other demographic information. Thus, the safety indices would apply to all drivers. We show that the less safe a driver is, the more frequently the driver needs to transmit information to the network. Furthermore, by adapting our communications algorithm for different drivers varying needs, we send only the most critical packets, opening up more capacity for the dissemination of higher priority messages and hence further improving safety of driving. Therefore, in our design, the transmission probabilities will be dictated by the safety indices of the drivers on the roadway (Fig. 3). Both deriving and employing the safety indices of drivers play key roles in the individualization algorithms, which are required to be efficiently run using limited computing resources on the vehicles.

Therefore, in this dissertation:

- We propose a method to estimate the PRT distribution of the drivers in Chapter 1.
- We propose an algorithm that reduces collision probability in the network by tuning the vehicular communications to the drivers' needs in Chapter 2.
- One of the most important factors in deriving the packet success is the assumed wireless communication interference. Hence, different interference models for VANETs and their effect on safety factors are studied in Chapter 3.
- At last, we analyze a similar type of ad hoc network (unmanned aerial vehicles) in order to find the acceptable range of intensity in Chapter 4.

CHAPTER 1

REAL-TIME ESTIMATION OF THE DISTRIBUTION OF BRAKE RESPONSE TIMES FOR AN INDIVIDUAL DRIVER USING A VANET

The effectiveness of warnings depends on how much time the driver needs to react. Therefore, to be as effective as possible, accident warning systems should be tailored to the specific characteristics of the driver. An important aspect of the specific characteristics of the driver is her distribution of brake response times (BRT). The BRT is the time elapsed between a stimulus such as a lead car braking or traffic signal changing color and a braking response by the driver. Since existing accident warning algorithms do not use the BRT distribution of individuals, drivers with different BRT in the same scenario receive the same warnings. Clearly, this approach is not optimal for the design of safety systems. The most important contributions of this chapter are:

1. Proposing a method for real-time estimation of the distribution of brake response times for an individual driver using data from a VANET system which has information about the positions, velocities, and accelerations of cars on the roads, road configurations, and the status and position of traffic signals.

2. Using the estimated distribution to customize warning algorithms to an individual driver's characteristics which leads to improvement in accident warning systems. We also study the trade-off between the false alarm rate and the accident probability of a vehicle and illustrate that at the same false alarm rate,

the accident probability may be lower by a factor of two when the estimated distribution is employed.

The chapter is organized as follows. In section 1.1, we review the relevant literature formally defining the BRT and related quantities, discussing factors that affect drivers' BRTs, and outlining several methods that have been proposed to estimate a driver's BRT. Section 1.2 outlines methods that can be used to estimate BRTs and what the distribution of a driver's BRTs would be if she did not intentionally delay braking.

1.1 Related Work and Basic Ideas

The time required to respond to a stimulus can be divided into several distinct phases. One such division is given by Koppa [39]. He defined the perception-reaction time or brake reaction time as the time required to perceive and initiate a reaction to the stimulus. In this chapter, we define the potential brake response time (PBRT) as the time in which a driver could have braked if she did not choose to delay braking, which is the relevant quantity for the purposes of an accident warning system. We will use the term "brake response time" (BRT) to refer to the observed quantity, the time elapsed between a stimulus such as a traffic signal color change and when the driver applies pressure to the brake pedal. These definitions are illustrated in Fig. 1.1. The estimation of BRT and PBRT both present technical difficulties. We review methods that have been proposed to estimate these quantities by previous researchers in the next subsections. Virtually every study to examine reaction times has found that the population distribution of reaction times is skewed right and several have shown that it is well approximated by a lognormal distribution [39], [24], [35]. We will make use of this fact later in our data analysis. The main ideas we build upon in this chapter were proposed by Zhang and Bham [35]. Their method is based on intuitive reasoning about the relationships between the distances, speeds, and accelerations of two cars when the following car reacts to an action taken by the lead car. The starting point

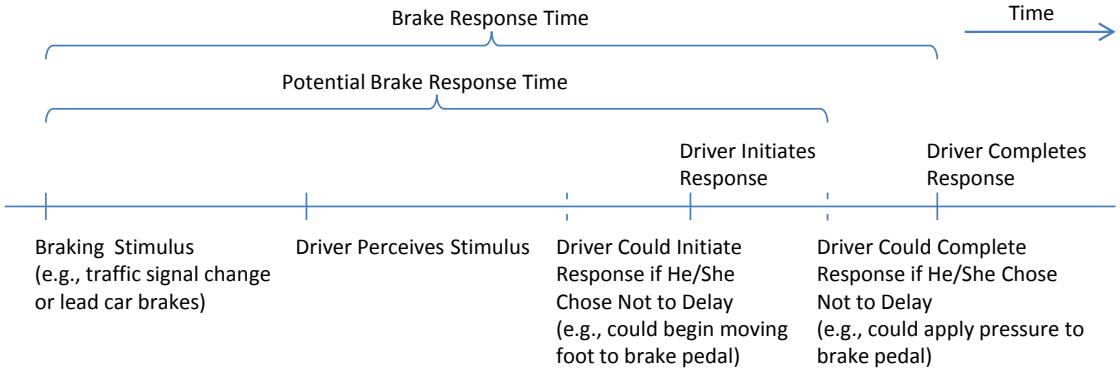

Figure 1.1: An illustration of the potential brake response time and brake response time.

in their algorithm is to identify two cars that go for a period of at least 4 seconds in which they are separated by less than or equal to 250 feet and their speeds are within 5 ft/s, or 1.52 m/s. These cars are said to be in a steady state. They then observe a time A when the distance between the cars decreases or increases while the follower has an acceleration rate of $\leq 0.5\text{ft/s}^2$. This change in distance between the cars is caused by acceleration or deceleration of the leader. Next they find the time B when the follower decelerates or accelerates at a rate $> 0.5\text{ft/s}^2$. The difference between times A and B is then an estimate of the follower's BRT. The advantages of this method are that it is intuitively reasonable, relatively easy to implement, and it yields reasonable reaction time estimates. However, the requirement that the cars be in a steady state is restrictive. To obtain more information about drivers' reaction times, it would be helpful to extend this approach to estimate reaction times in situations other than the steady state.

Another method for BRT estimation was proposed by Ma and Andréasson and is based on techniques designed to find the lag between two linearly related time series [42]. The basic idea of the method is to examine the covariance between the time series in the frequency domain, as measured by the coherency. However, this

method does not allow us to estimate separate BRTs to separate events in a natural way.

A third approach was taken by Ahmed, who specified a reaction time distribution as part of a larger model of car-following behavior, and estimated all parameters of this model jointly through maximum likelihood techniques [43]. However, the maximum likelihood estimates had to be obtained numerically, which is computationally intensive due to the complexity of the model. Therefore, this method would not be practical to implement in an accident warning system where the BRT distribution must be obtained with limited computing resources. Furthermore, one of the desired requirements for the warning systems is to use the individual perception reaction time data online. In other words, the model needs to become more accurate as more information becomes available from VANET system. However, based on most of the current methods we cannot update the algorithm in real-time. Three previous studies have addressed the problem of estimating the distribution of "true" reaction times based on observed brake response times. All of these studies examined this problem in the context of traffic signals, and focused on estimation of population distributions rather than distributions of response times for a particular individual. Goh and Wong take a more sophisticated approach [24]. They define a transitional zone (TZ) based on the time headway (i.e. a measurement of the time in which the vehicle arrives at the traffic signal without the reduction in the speed) between the driver and the traffic signal at the time that it changes to yellow. This TZ is "an empirically calibrated range of time headways suitable for identifying drivers with realistic stop-or-cross decisions" [24]. Essentially, to estimate response times, they limit the sample to those cars with a time headway of ≤ 4 seconds. Nearly all cars that chose not to stop at the light were within the 4-second threshold; thus, this threshold includes cars with a "real" choice between stopping and continuing on. However, by restricting the sample to those cars within the TZ, they lose the information contained in those other

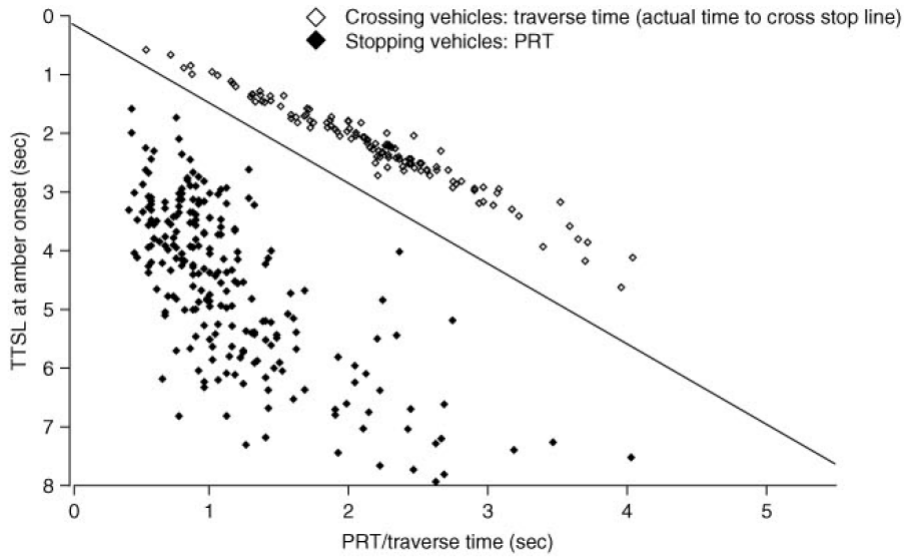

Figure 1.2: Plot from Goh and Wong [24] of observed brake reaction times (PRT in their terminology), the dependent variable, vs. time headway to traffic signal, the independent variable. Points above the diagonal line correspond to cars that did not stop at the intersection. This figure shows a subset of the data later employed in this chapter.

data points. This is a particularly critical problem in our application, where we wish to learn about response times for a particular driver. We may not have the chance to observe response times very frequently for a single driver; it would therefore be helpful to be able to use all observed data points rather than just those with a time headway of 4 seconds or less.

1.2 Estimating the Distribution of Potential Brake Response Times

1.2.1 General Discussion

In this section, we discuss the construction of a statistical model for the distribution of brake response times and how this model can be used to estimate the distribution of potential brake response times for a particular individual. We adopt a lognormal model for brake reaction times, modeling the logarithm of the observed

BRT as normally distributed conditional on the time headway. This lognormal model also has the advantage of automatically correcting for some differences in the variance of the BRT distribution at different time headways and across individuals. Goh shows that as the time headway increases, the mean BRT and the variance of the BRTs both increase [24]. Similarly, it seems likely that some individuals have lower or higher mean reaction times than other drivers, and that the variance in the BRT distribution varies across individuals as well. Specifically, it is likely that individuals with a low mean reaction time also have a low variance in their reaction times, whereas individuals with a high mean reaction time also have a high variance in their reaction times. These differences in the variance of brake reaction times will be approximately corrected by modelling the logarithm of the BRT. It also seems likely that the mean and variance of the brake response time distribution depend on several other variables. An important factor that will be accounted for in our model is the stimulus type (e.g. traffic signal vs. lead car decelerates). Reaction times also depend on a large number of other factors such as weather conditions and demographic characteristics of the driver. However, these variables will not generally be available to the accident warning system, so their effects will be absorbed into the error term of our model.

1.2.2 The Model

Using just the time headway as an explanatory variable, the general ideas above can be formalized in the following model:

$$\begin{aligned} \mathbf{y}_d &\sim N(X\beta + X\gamma_d, \sigma^2 I) \\ \gamma_d &\sim N(0, \Sigma_\gamma) \end{aligned} \tag{1.1}$$

In this model,

- d indexes the driver

- $\mathbf{y}_d$ is a vector of the logarithms of observed reaction times for a particular driver.
- X is a matrix of covariates, detailed further below.
- β is a fixed vector of unknown coefficients.
- σ^2 is an unknown scalar.
- γ_d is a random vector of unknown coefficients.
- Σ_γ is an unknown matrix.

The basic idea of this model is that, conditional on the time headway, the distribution of BRTs for an individual driver has a mean which is given by an overall population mean, $X\beta$, plus an offset due to the particular characteristics of that driver, $X\gamma_d$. This is illustrated in Fig. 1.3. It is assumed that the parameters γ_d determining the individual's offset to the overall mean follow a multivariate Normal distribution in the population. This is a linear mixed effects model [44]. A key assumption made in this model specification is that after the log transformation, the covariance matrix $\mathrm{Cov}[\mathbf{y}_d]$ has the simple form $\sigma^2 I$. This assumption could fail to hold in a number of ways, but it makes the calculations much easier. The final results (Fig. 1.5) show the estimation is sufficiently accurate as long as sufficient number of samples are employed.

Since the logarithm is a monotonically increasing function, it follows that the logarithm of the BRT is also an increasing function of time headway. For flexibility, we allow the possibility that the log BRTs are a quadratic function of time headway. We also allow for the possibility that the relationship between time headway and BRT is slightly different for each of the different stimulus types. For instance, it could be that drivers have a faster BRT at low time headways and the average BRT increases more rapidly as a function of time headway when the stimulus is a lead car braking

than when it is a traffic signal changing to yellow. These considerations lead to the following possible form of the mean log-BRT as a function of time headway:

$$E[y_{dsi}] = \beta_{s,0} + \beta_{s,1} t_{dsi} + \beta_{s,2} t_{dsi}^2 + \gamma_{d,s,0} + \gamma_{d,s,1} t_{dsi} + \gamma_{d,s,2} t_{dsi}^2 \tag{1.2}$$

In Equation (1.2), d indexes the driver, s indexes the stimulus type, and i indexes the observation (so if we have 5 different BRT observations for a particular driver and stimulus type, i will vary from 1 to 5). As before, y_{dsi} is the log brake reaction time, and t_{dsi} is the time headway at the time of the stimulus. The subscript s on the β and γ terms indicate that the values of those coefficients depend upon the stimulus type s. To make this concrete, if this mean function is adopted and there are $S = 3$ different stimulus types under consideration with n_{ds} observations for driver d under stimulus type s, β and γ_d are 9×1 vectors and the portion of the X matrix corresponding to observations for driver d will be of the following form:

$$\begin{bmatrix}
1 & t_{d11} & t_{d11}^2 & 0 & 0 & 0 & 0 & 0 & 0 \\
1 & t_{d12} & t_{d12}^2 & 0 & 0 & 0 & 0 & 0 & 0 \\
\vdots & \vdots & \vdots & \vdots & \vdots & \vdots & \vdots & \vdots & \vdots \\
1 & t_{d1n_{d1}} & t_{d1n_{d1}}^2 & 0 & 0 & 0 & 0 & 0 & 0 \\
0 & 0 & 0 & 1 & t_{d21} & t_{d21}^2 & 0 & 0 & 0 \\
\vdots & \vdots & \vdots & \vdots & \vdots & \vdots & \vdots & \vdots & \vdots \\
0 & 0 & 0 & 1 & t_{d2n_{d2}} & t_{d2n_{d2}}^2 & 0 & 0 & 0 \\
0 & 0 & 0 & 0 & 0 & 0 & 1 & t_{d31} & t_{d31}^2 \\
\vdots & \vdots & \vdots & \vdots & \vdots & \vdots & \vdots & \vdots & \vdots \\
0 & 0 & 0 & 0 & 0 & 0 & 1 & t_{d3n_{d3}} & t_{d3n_{d3}}^2
\end{bmatrix}$$

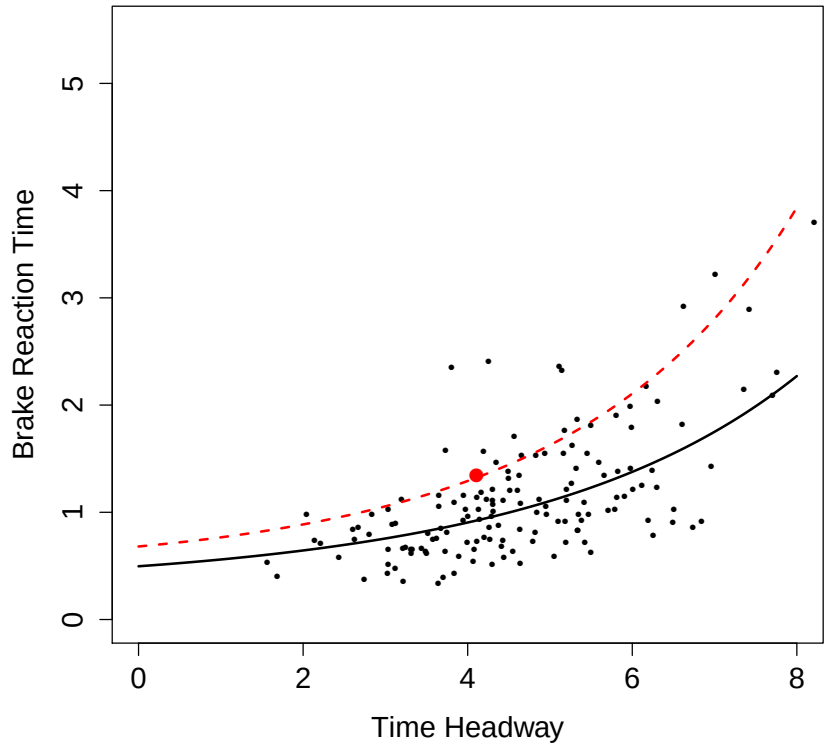

Figure 1.3: An illustration of the model based on a simulated data set provided by [24]. The plot shows simulated data for just one stimulus type. The black curve represents the population-average relationship between time headway and brake reaction time, $X\beta$. The red curve represents the relationship between time headway and brake reaction time for one individual, $X(\beta + \gamma)$. The red point is an observation for that driver.

1.2.3 Training the Model: A Fit Using Data from Driving Simulations

For training the model, the data are gathered for D subjects in a driving simulation. We prefered to gather data from real drivers on the road, but this was likely to be too difficult to be feasible. This being the case, we took precautions to address concerns about using results from a driving simulation to learn about response times for drivers in real life driving situations. The subjects in the study were a representative sample of the overall population of drivers who were using the accident warning system. Brake responses for each subject were elicited at a variety of levels of expectancy.

To improve the statistical analysis, responses were also collected at a range of time headways for each stimulus type. To separate the effects of expectancy and any other variables that may be included in the model, the combinations of these factors were randomized (for example, we had some observations where the braking stimulus was more and less surprising at different levels of the time headway variable). For each driver, we have multiple observations of reaction times for each stimulus type. These data can be used to estimate the unknown quantities β, σ^2, and Σ_γ in this model using standard statistical techniques implemented in the lmer function of the lme4 library in R. We will use a subscript of (tr) to indicate quantities obtained from this training data set; in particular, let $X_{(tr)}$ be the covariate matrix obtained using data from this data set and denote the estimates by $\widehat{\beta}_{(tr)}$, $\widehat{\sigma}^2_{(tr)}$, and $\widehat{\Sigma}_{\gamma(tr)}$. $\widehat{\beta}_{(tr)}$ can be written as

$$\begin{aligned}
\widehat{\beta}_{(tr)} &= (X'_{(tr)}V^{-1}_{(tr)}X_{(tr)})^{-}X'_{(tr)}V^{-1}_{(tr)}\mathbf{y}_{(tr)} \\
V_{(tr)} &= \mathrm{Cov}(\mathbf{y}_{(tr)}) = X_{(tr)}\widehat{\Sigma}_{\gamma(tr)}X'_{(tr)} + \widehat{\sigma}^2_{(tr)}I. \qquad (1.3)
\end{aligned}$$

The superscript $''-''$ denotes a generalized inverse. The estimates $\widehat{\sigma}^2_{(tr)}$ and $\widehat{\Sigma}_{\gamma(tr)}$ were found through numerical maximum likelihood techniques by employing different libraries (e.g. stats4) in R. A study conducted by McGehee et al. has found that the population average brake response time was about 0.3 seconds faster in driving simulations than it was in real life driving studies [45]. This difference was found at time headways of approximately 2 seconds. It is difficult to account for this effect in a rigorous way, especially since this observed difference may be due in part to methodological differences between the simulator trials and the real car driving trials. As an ad hoc solution, we increased the estimated value of $\widehat{\beta}_{0,(tr)}$ by an amount such that the estimated population mean reaction time at a time headway of 2 seconds was increased by 0.3 seconds.

1.2.4 Real Time Estimation of the PBRT Distribution for One Driver

We estimate the distribution of PBRTs for a particular driver in two steps. First, we establish the relationship between the covariates and BRT for that driver. Then we use this relationship to estimate the distribution of PBRTs by using values of the covariates at which the BRT does not include an intentional delay to braking.

1.2.4.1 Estimating the Relationship Between Time Headway and BRT for One Driver

As data are gathered in real time for an individual driver d^*, our goal is to estimate the driver's offset γ_{d^*} to the population-average regression coefficients β. This is estimated by the Best Linear Unbiased Predictor (BLUP) [37], [38]. Intuitively, we might expect that if a particular driver has a higher than average brake response time in one stimulus type, they are likely to have a higher than average brake response time in other stimulus types as well. Similarly, if they are particularly sensitive to the time headway in one situation, they are more likely to be sensitive to the time headway with other stimulus types. This intuition suggests that the covariance matrix Σ_γ will have non-zero off-diagonal entries; that is, there is some degree of correlation among the γ_d coefficients. Because of this correlation, observations from one stimulus type can give us information about the coefficients in the other stimulus types. For example, if we make some observations of driver brake response times in the traffic light setting which give positive estimates of the γ_d coefficients for that stimulus, a positive correlation between the coefficients might lead to positive estimates of the coefficients for other stimuli as well. To reduce the computational complexity of computing the BLUP, we assume that the information about the unknowns β, σ^2, and Σ_γ that is provided by the training data set from the driving simulator is much greater than the information provided by the data from this individual driver. That is, the estimates $\widehat{\beta}_{(tr)}$, $\widehat{\sigma}^2_{(tr)}$, and $\widehat{\Sigma}_{\gamma(tr)}$ obtained from the training data set above

are very similar to what we would obtain if we estimated them using the combined training data set with the observations for this driver. If this assumption holds (i.e. little information is obtained in real-time for the driver), we can approximate the BLUP using the estimates of these quantities found with the training data set, which saves the computational effort of re-fitting the model every time we observe a new reaction time. Let X_{d^*} be the covariate matrix X as in the full model, but formed using only the data from driver d^*. The BLUP of $\hat{\gamma}_{d^*}$ is

$$\hat{\gamma}_{d^*} = \widehat{\Sigma}_{\gamma(tr)} X'_{d^*} \widehat{V}_{d^*}^{-1} (\mathbf{y}_{d^*} - X_{d^*} \widehat{\beta}_{(tr)}), \tag{1.4}$$

where $\widehat{V}_{d^*} = X_{d^*} \widehat{\Sigma}_{\gamma(tr)} X'_{d^*} + \widehat{\sigma}^2_{(tr)} I$. The covariance matrix of the BLUP $\tilde{\gamma}_{d^*}$ is given by

$$\mathrm{Cov}(\tilde{\gamma}_{d^*}) = \Sigma_\gamma X'_{d^*} V_{d^*}^{-1} (V_{d^*} - X_{d^*} \mathrm{Cov}(\widehat{\beta}_{(tr)}) X'_{d^*}) V_{d^*}^{-1} X_{d^*} \Sigma_\gamma \tag{1.5}$$

To estimate the covariance matrix of $\hat{\gamma}_{d^*}$, we plug our approximation (Equation 1.3), to $\widehat{\beta}_{(tr)}$, and our estimates of σ^2, Σ_γ, and $\mathrm{Cov}(\widehat{\beta}_{(tr)})$ into Equation 1.5. When no data have been gathered yet, the best predictor is just the vector 0, with covariance matrix Σ_γ. In this case, the estimated mean for the individual is equal to the estimated mean for the population of all drivers.

1.2.4.2 Obtaining the Estimated PRBT Distribution

The final step is to estimate the distribution of potential brake response times for an individual driver, not including any delays. For the suggested model form above using a quadratic function of time headway, the intuitive idea is to pick a specific time headway value t^* at which the driver does not have enough time to delay braking, and use that time headway value to evaluate the mean function. Based on the plots in [24] (Fig.2), it appears that $t^* = 1.5$ seconds might be an appropriate value (there is no vehicle in this interval $[0, 1.5]$ who delays the braking). We can then estimate the

mean of the driver's log-RTs by plugging $t^* = 1.5$ seconds into the estimated mean function: $\hat{\mu} = \hat{\beta}_0 + \hat{\gamma}_{d^*,0} + t^*(\hat{\beta}_1 + \hat{\gamma}_{d^*,1}) + (t^*)^2(\hat{\beta}_2 + \hat{\gamma}_{d^*,2})$. This provides an estimated mean for the log-reaction time. There are several options for estimating the variance of the log-PBRT distribution. One simple idea would be to use the estimate $\widehat{\sigma}^2_{(tr)}$ of the quantity σ^2 in the model statement 1.1. However, this does not take into account the uncertainty in our estimate $\hat{\mu}$. This uncertainty is captured by the prediction error, $(\widehat{\beta}_{(tr)} + \hat{\gamma}_{d^*}) - (\beta + \gamma_{d^*})$. It can be shown that $\text{Cov}((\widehat{\beta}_{(tr)} + \hat{\gamma}_{d^*}) - (\beta + \gamma_{d^*})) = \text{Cov}(\widehat{\beta}_{(tr)}) + \text{Cov}(\hat{\gamma}_{d^*} - \gamma_{d^*}) - \text{Cov}(\widehat{\beta}_{(tr)}, \gamma'_{d^*}) - \text{Cov}(\gamma_{d^*}, \widehat{\beta}_{(tr)})$, where

$$\text{Cov}(\hat{\gamma}_{d^*} - \gamma_{d^*}) = \Sigma_\gamma - \text{Cov}(\hat{\gamma}_{d^*}) \tag{1.6}$$

$$\text{Cov}(\hat{\gamma}_{d^*}) = \Sigma_\gamma X'_{d^*}(V^{-1}_{d^*} - V^{-1}_{d^*} X_{d^*} \text{Cov}(\widehat{\beta}_{(tr)}) X'_{d^*} V^{-1}_{d^*}) X_{d^*} \Sigma_\gamma \tag{1.7}$$

$$\text{Cov}(\widehat{\beta}_{(tr)}, \gamma'_{d^*}) = \text{Cov}(\widehat{\beta}_{(tr)}) X'_{d^*} V^{-1}_{d^*} X_{d^*} \Sigma_\gamma \tag{1.8}$$

This covariance can be estimated by plugging in estimates of the unknown quantities V_{d^*}, $\text{Cov}(\widehat{\beta}_{(tr)})$, and Σ_γ. An estimate of the variance of the distribution of log-PBRTs which takes into account our uncertainty about the value of the mean is then

$$\begin{bmatrix} 1 & t^* & t^{*2} \end{bmatrix} \widehat{\text{Cov}}((\widehat{\beta}_{(tr)} + \hat{\gamma}_{d^*}) - (\beta + \gamma_{d^*})) \begin{bmatrix} 1 & t^* & t^{*2} \end{bmatrix}' + \hat{\sigma}^2_{(tr)}$$

When we do not yet have any data, the adjusted variance estimate is

$$\begin{bmatrix} 1 & t^* & t^{*2} \end{bmatrix} \widehat{\Sigma}_\gamma \begin{bmatrix} 1 & t^* & t^{*2} \end{bmatrix}' + \hat{\sigma}^2_{(tr)}. \tag{1.9}$$

Fig. 1.4 shows the resulting distribution estimates obtained in a simulation when these variance estimates are used as the parameters of the distribution of PBRTs. We used the same samples available for Goh's research to estimate the PBRT distribution (e.g. for Fig. 1.2). From this plot we can see that the estimates taking into account uncertainty in the coefficient estimates are more conservative. On the scale of these

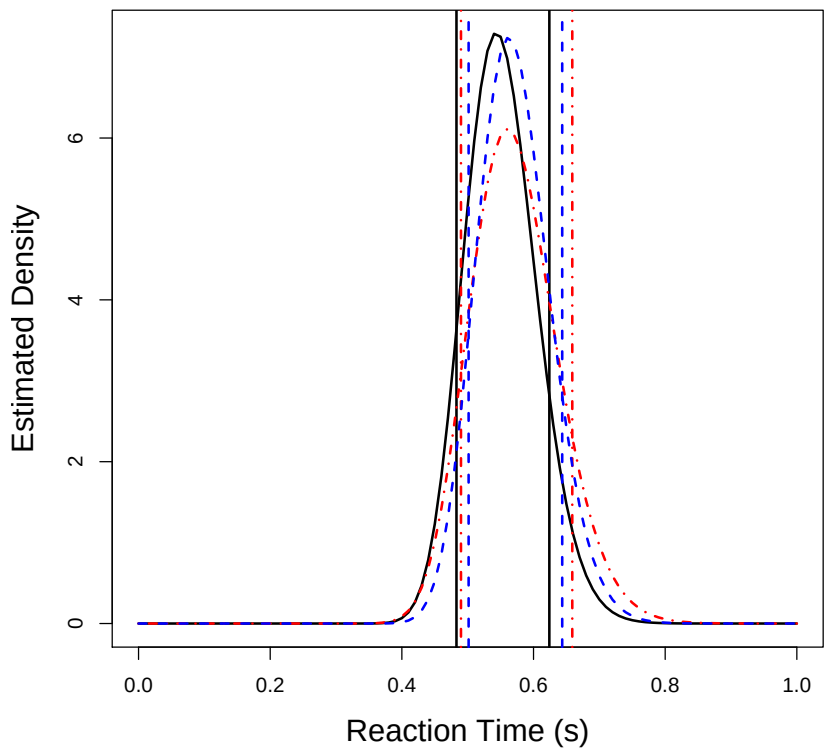

Figure 1.4: Estimates of the distribution of PBRTs for an individual obtained in a simulation. The black curve represents the individual's "true" response time distribution. The blue curve is the estimated distribution when the variance is taken to be $\hat{\sigma}^2$. The red curve is the estimated distribution when the variance estimate includes a term for uncertainty in $\widehat{\beta}$ and $\widehat{\gamma_{d^*}}$. The vertical lines are at the 10th and 90th percentiles.

simulation results, the difference in the percentiles obtained from these estimates is just a fraction of a second, but the difference could be more significant with real data. We will use the more conservative value for the estimated variance since it more accurately reflects what we know about the distribution of response times based on the available data. Fig. 1.5 shows how the estimated reaction time distribution changes with the sample size and the allocation of the sample among the different stimulus types. These results are dependent upon the parameter values used in the simulation, but they illustrate that observed reaction times for the stimulus type that is used in

estimating the PBRT distribution contribute more information than observations in other stimulus types.

We note that computation of the estimated PBRT distribution requires only the operations of matrix inversion and matrix multiplication. The matrix which must be inverted is $\widehat{V}_{d^*}$, which has dimension $n_{d^*} \times n_{d^*}$, the number of observations for driver d^*. The inversion operation has computational complexity $O(n_{d^*}^3)$. All of the matrix multiplication operations are between matrices of dimension 9×1, 9×9, $9\times n_{d^*}$, $n_{d^*}\times1$. Because multiplying an $n \times m$ matrix by an $m \times k$ matrix has complexity $O(nmk)$, this implies that the complexity of the "worst" matrix multiplication operation is $O(9n_{d^*}^2)$ (for the product $X'_{d^*}\widehat{V}_{d^*}^{-1}$). Therefore, the whole computation has complexity $O(n_{d^*}^3)$.

1.2.5 Estimated PBRT Distribution vs Population Distribution

In this section, our goal is to relate the estimated individual distribution to the distribution of BRTs for the population in order to show how accident warning algorithms benefit from taking the estimated distribution into account. As discussed earlier, researchers have consistently found that reaction times are skewed right and are approximated well by a lognormal distribution. It is reasonable to assume that brake reaction times are skewed right within individuals as well. As we mentioned, [39] established that the distribution of BRTs of drivers reacting to surprise events follows a log-normal curve with parameters $\mu = 0.17$ and $\sigma = 0.44$ (the population distribution). We try to minimize the frequency of false alarms that the system gives subject to this distribution. If the system detects that the driver has less than his or her BRT to react to an obstacle, it should give the driver a warning. We can only state the probability that any BRT is above or below a certain value. Thus, the constraint states that we must calculate some threshold T_t above which there is only small chance a BRT can be, and send a warning whenever a driver has less than

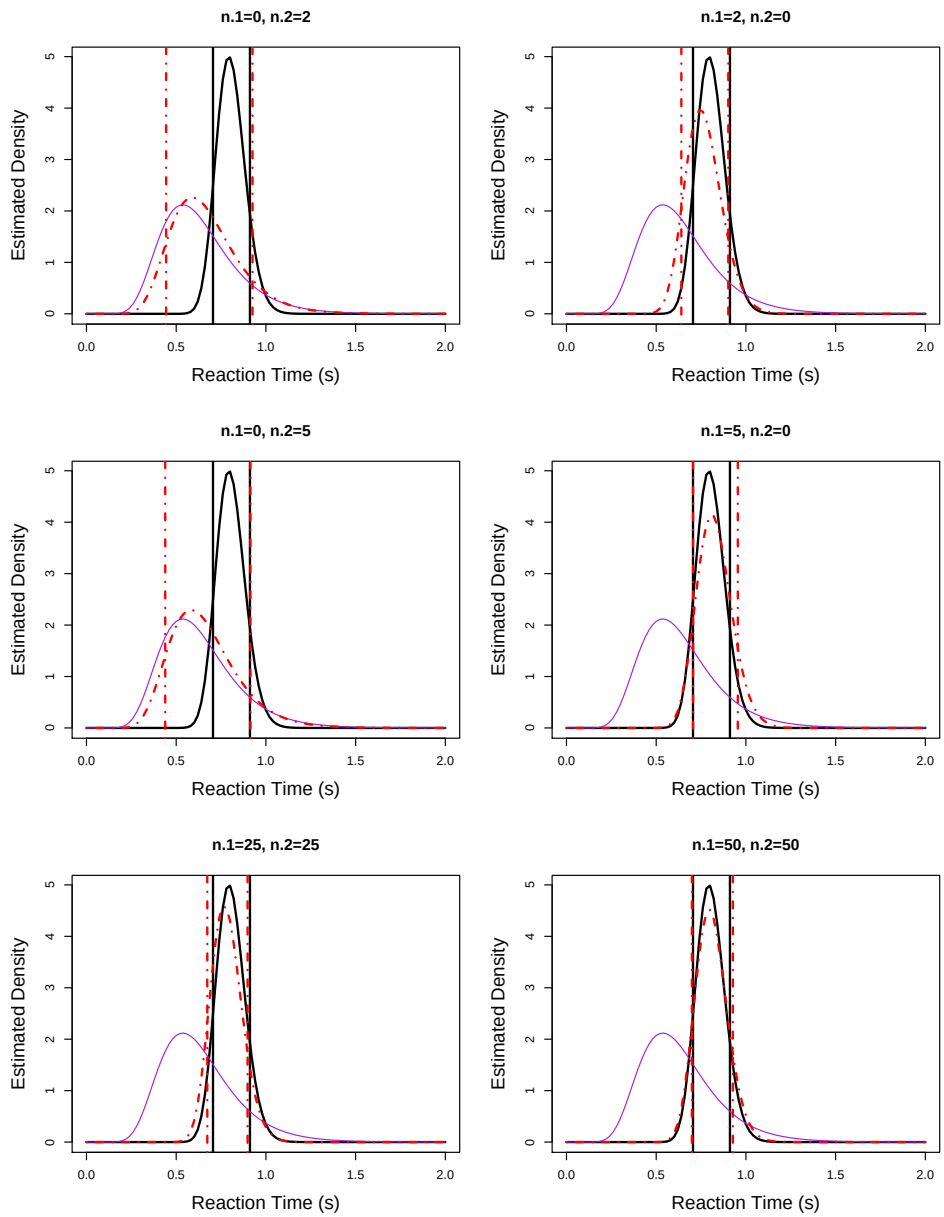

Figure 1.5: Estimates of the distribution of PBRTs for an individual obtained in a simulation with different sample sizes. $n.1$ and $n.2$ represent the number of observations for stop light and car braking stimuli for one driver respectively. The black curve represents the individual's "true" response time distribution. The purple curve represents the distribution of reaction times in the population, which is used as an estimate when the sample size is 0. The red curve is the estimated distribution. The vertical lines are at the 10th and 90th percentiles.

this amount of time to react. Therefore, we can calculate the threshold to send the warnings using the distribution for the entire population:

$$P(Y \leq T_t) = \Phi\left(\frac{\ln(T_t) - 0.17}{0.44}\right) = 1 - \text{prob. of accident} \tag{1.10}$$
$$\Phi(x) = \frac{1}{\sqrt{2\pi}} \int_{-\infty}^{x} e^{\frac{-t^2}{2}} dt$$

Also, we can calculate the warning threshold using the distribution for an individual driver (black curve in Fig. 1.4).

Now that we have established the thresholds for sending accident warnings, we can calculate the false alarm rates that will result from employing these two different systems. A false alarm occurs whenever a warning is sent, but it is not needed. To best explain this problem, let us consider a scenario in which a vehicle is following another vehicle on a one-lane roadway when the lead vehicle suddenly begins to decelerate to avoid an unexpected obstacle. Suppose that the system has calculated that the following driver has t seconds to react, and that t is less than T_t, therefore a warning has been sent. Then, the false alarm rate is the probability that the driver's reaction time, X will be less than t. Therefore, $F_X(t)$, the cumulative distribution function is the total false alarm rate. Fig. 1.6 illustrates false alarm rate versus probability of accident for different errors in estimating the individual distribution by using the real data. It is clear from Fig. 1.6 that when we use the population brake reaction distribution, the false alarm rate can be higher by almost a factor of two than when we use the individual driver's distribution. Therefore, in this scenario, safety applications could potentially take full advantage of being customized to an individual's characteristics.

1.3 Conclusion

Accident warning systems generally rely solely on the distribution of the entire population of drivers, thereby ignoring the distinct characteristics of individual drivers. They may frustrate the drivers with the overly high numbers of false alarms, causing them to ignore warnings or even disable the system. If drivers are distracted

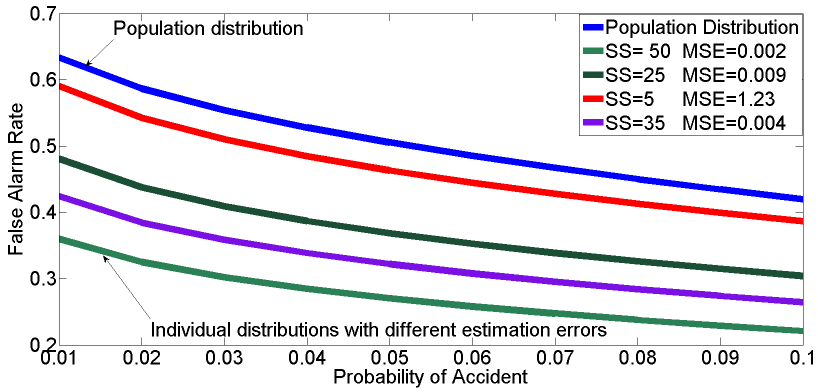

Figure 1.6: Plotting Equation 1.10 using MATLAB. This figure shows the false alarm rate (y axis) versus the probability of accident (x axis), the percentage of possible accidents that the system fails to give warning about, using population and individual PBRT distributions. Population distribution = $lnN(0.17, 0.44^2)$, based on results from [39]. SS represents the sample size equally considered for the two scenarios and MSE shows the mean square error of the estimated distributions.

by overly frequent warnings, the safety benefits of the system are compromised or even lost. In this chapter, we discussed the need to adapt accident warning systems to drivers' individual characteristics and proposed a method as the first step for doing this customization by estimating the distribution of potential brake response times for an individual driver in real time. We showed that at the same accident probability for each driver, the false alarm rate can be reduced by at least 30% by employing the estimated individual distribution instead of the population distribution.

CHAPTER 2

PACKET SUCCESS PROBABILITY DERIVATION FOR THE CUSTOMIZED DESIGN

Let us assume the scenario in which a chain of moving vehicles exists in one lane. As we discussed, a major cause of accidents is the slow response time of drivers to stopped traffic. In order to improve drivers' safety using personalized vehicular communications, first we need to know the delay requirements of the safety applications. In general, the difference between the communication delay of the desired transmission and the sum of perception reaction times of drivers in a chain plays the main role in reducing the average collision probability of the vehicles.

Next, we need to know about the success probability of the packet delivery between two specific vehicles while other vehicles might also transmit simultaneously, thus interfering with the selected packet transmission. Deriving this probability helps us with finding the communication delay to inform each vehicle in a chain while employing vehicular communications. It is desirable to reduce this delay as much as possible by lessening the interference caused by other vehicles. Our proposed algorithm tunes this transmission probability of each vehicle based on the individual characteristics of drivers and the traffic conditions around the vehicles.

Our main contributions in this chapter are as follows:

1. We propose a customized MAC layer design in order to reduce the number of collisions on highways.

2. We find the expression of packet success probability for two specific scenarios regarding a chain of vehicles on a highway.

3. We find the approximated required channel access probabilities equations.

4. We illustrate the collision probability reduction by at least 25% for the specified models using Monte Carlo simulations.

The remainder of this chapter is organized as follows. Section 2.1 summarizes the related work that has been done in the field of vehicular communications regarding improving drivers' safety and driver behaviour detection. We propose our novel MAC level design with respect to personalized vehicular communications to avoid vehicle collisions in section 2.2. Section 2.3 presents the algorithm for customizing channel access probabilities in VANET. In section 2.4, the simulation and numerical results are demonstrated to verify the effectiveness of the proposed scheme.

2.1 Background and Literature Review

We aim at customizing VANET by changing the communications parameters in a smart way. None of the related works actually have proposed a MAC level design to tune the VANETs to drivers and traffic conditions for safety applications. We proposed a regression method to estimate drivers' PRTs distributions using VANET (Chapter 1). Also, Al-Sultan et al. [5] utilized Bayesian graphical models to detect drivers' behaviors and categorize them. However, these two papers only focused on estimating the PRT of drivers and deriving an index for a driver, respectively. They did not propose any algorithm to use the driver's index or any other factor in individualizing vehicular communications. Also, we showed in Chapter 1 how using an individual driver's PRT distribution in order to individualize warnings results in an impactful reduction in the probability of the driver not being able to brake in time. However, that paper only took the PRTs distribution of drivers into account to customize warnings to the drivers. In other words, it employed the estimated perception reaction time after the vehicle receives the safety messages. It does not analyze how

channel access probabilities of vehicles and vehicular communications can be adapted to drivers' characteristics and traffic conditions. Besides, the vehicles' collision probability were assumed to vary in a specific range in Chapter 1 because only the trade-off between vehicles' collision probabilities and the false alarm rates were discussed for two types of collision warning systems. Jiafu et al. [7] presented context-aware vehicular clouds in which vehicles act as cloud service providers and clients. However, they did not propose any specific design to improve safety. Moreover, they discussed their proposed methods briefly in theory without providing sufficient detail on the implementability of them. In contrast, our context-aware approach takes advantage of tuning MAC-level communication parameters to lower the vehicles' collision probability. Haas et al. [8] simulated two vehicular safety applications and determined the effect of various communication parameters on vehicle crash avoidance through simulations. However, they did not develop any mathematical framework for safety requirements of VANET. Also, they neglected the fact that different drivers face different needs. Therefore, their simulation-based study both could not achieve the potential decrease in the number of collisions and waste the communication resources. Qian et al. [9] proposed a MAC protocol for vehicular communications with different message priorities. However, their study was only focused on security aspects of safety applications and does not attempt to reduce the number of collisions. Mughal et al. [10] evaluated transmission rate or power control techniques which were employed to control congestion in dense traffic. There is no mathematical framework presented in [10]. It suggested the combination of transmission rate and transmission power control methods would be more efficient as a congestion control mechanism only in theory. Chang et al. [11] proposed a series of repetition-based Media Access Control (MAC) protocols to deliver periodic status updates within their useful lifetime to within a specified range. For a scheme in which nodes transmit with a given probability in each slot, Chang et al. [11] derived the Probability of Reception

Failure (PRF) at the border of the range of interest. However, they only considered the strongest interferer in their derivation and neglect fading. The authors did not mention how their design meets the specific packet reception probabilities and delay requirements that are associated with the different driver safety characteristics in general or the specific safety information demands of a given situation in which a collision may be imminent. Garcia-Costa et al. [12] developed a stochastic model in which they derived the average number of collisions (when the leading vehicle stops instantly) in a chain of vehicles that are equipped with a collision warning system. The operation of the communications system was abstracted by a message delay variable whose distribution was assumed given for any specific MAC scheme. Moreover, it was assumed that all vehicles in the chain receive the warning message at the same time. Neither of these assumptions seem realistic. Carbaugh et al. [13] compared the safety of automated and manual highway systems with respect to rear-end collision frequency and severity. Yet, they assumed a fixed communications delay of 300, 150, and 120 milliseconds for autonomous, low-cooperative, and high-cooperative vehicles, respectively, an assumption which might not be realistic. Furthermore, Darus et al. [22] and Sattari et al. [23] both categorized and proposed different congestion control algorithms. Most of these algorithms were efficient based on message priorities. They nevertheless ignored the drivers' characteristics completely. In addition, it is not well-specified how these priorities are defined. To wrap this section up, none of the previous studies have actually proposed a MAC level design for employing both the drivers' behaviour and traffic information in order to improve safety.

In the next sections, we will show that by taking the estimate of drivers' behaviours and traffic data into account, vehicular communications can be tailored to the needs of drivers and the network (Fig. 3). Therefore, while each vehicle increases its level of safety by obtaining additional information from the network, it transmits valuable data to other vehicles especially before it causes danger to others. As a vital

result, the number of fatalities on highways will be decreased.

2.2 Driver-based Adaptation of Vehicular Communications

Communications between vehicles can help decrease collisions in an N-lane highway. It can help drivers with making proper reactions to the deceleration events especially when a driver cannot either observe or perceive the deceleration of other vehicles due to low visibility, high unexpectedness of the incident, defective brake lights, and many distractions that nowadays exist on the roads. In a network of vehicles, each vehicle transmits with a specific probability in the transmission medium. Large channel access probabilities lead the system to excessive interferences and consequently low probability of packets being successfully received (success probability) while very small values reduce the success probabilities since the probability of the favorite transmission is low itself. Therefore, there is an optimized value given both the physical data (distances, velocities, and deceleration rates) obtained by vehicular networks and the communications protocol requirements, which results in lower collision probability of vehicles than when the non-optimal access values are employed for the vehicles. Now, can we achieve even lower collision probabilities by customizing the VANET communications? In section 2.4, it is shown that there could be individualized channel access probabilities for different vehicles leading to even lower collision probability. Our main idea is that unsafe vehicles need to inform other vehicles of their perilous situation more frequently than safer vehicles, i.e, with higher channel access probability. Our simulation results confirm this assumption which will be discussed in the following section.

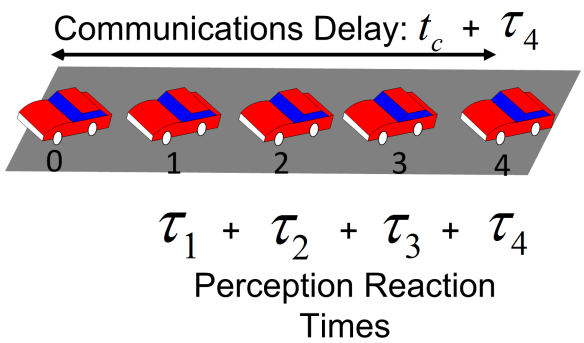

Figure 2.1: Communications delay versus sum of PRTs. This figure illustrates the time before a driver in a chain applies the brake.

2.2.1 Delay Requirements of the Safety Application

Consider a traffic stream where a chain of vehicles move with constant speed v and randomly chosen inter-vehicle spacing. When V_0 (the first vehicle in the chain) brakes, the driver of V_1 (the following vehicle), after her PRT, τ_1, applies the brake. Having no inter-vehicle communications employed, vehicle V_i $(i > 1)$ applies the brake after $\sum_{j=1}^{i} \tau_j$, the sum of PRTs up to the driver i. With the communications, this time will change to $\tau_i + t_{c_i}$ in which t_{c_i} is the communications delay to inform vehicle V_i. Note that t_{c_i} can be a result of direct communications from V_0 to V_i or the retransmission of V_0's signal by one of the vehicles in the middle. Understandably, when $t_{c_i} < \sum_{j=1}^{i-1} \tau_j$, which is almost always the case especially in critical scenarios, V_i has more time to react and as a result the collision probability is reduced (Fig. 2.1).

2.2.2 Analysis and Design

May et al. [14] states that the traffic of vehicles is more likely to follow Poisson distribution under low flow conditions. Under near-capacity conditions, however, the equal distance assumption between vehicles is justified. It is noted in [14] that in a

dense and non-free traffic flow regime all drivers tend to maintain a constant spacing with their leader. Therefore, our design is divided into two cases: 1. Equal distance model 2. Poisson distribution model. We believe examining these two scenarios gives us a thorough picture of how vehicular communications can affect collision probability in general. The traffic model does not ignore congestion from intersecting roadways, however, we assume as new vehicles enter a highway our model is still preserved.

Although the Media Access Control (MAC) protocol for DSRC communications is a variation of the conventional CSMA/CA scheme, because of the short length of the packet payload and the broadcast nature of communications, the 4-way handshake anticipated by the standard is not efficient for the dissemination of periodic safety messages. RTS/CTS and ACK message exchanges increase the hidden node problem thus resulting in higher probability of packet collisions [16]. Since the topology of VANETs is highly dynamic, we need protocols which do not need a detailed description of the network topology to schedule packet transmissions. Repetition-based protocols not only reveal this property, but also fight packet collisions due to the problem of hidden nodes. Hence, in this section, we make use of repetition-based protocols for the dissemination of periodic safety messages. A similar approach has been used in other papers, e.g. in [17] and [16].

1. Equal distance:

   The MAC scheme that we consider is SSP (Slotted Synchronous P-persistent) where at each slot a node (vehicle) transmits with probability p and receives with probability $1 - p$ independent of others. The important assumption is that the slots are synchronized because of the on-board GPS devices. Moreover, since the vehicles are not faced with power constraints, the nodes can increase the transmission power to overcome the interference. In this chapter, we consider path loss and Rayleigh fading for formalizing the signal propaga-

tion characteristics. If we assume that the nodes transmit with unit power, the received power at distance r is $hr^{-\alpha}$, where $\alpha(> 1)$ is the path loss exponent and h is the fading coefficient.

Theorem:

Assuming that a node transmits a packet, the probability that a receiver at distance r on the same lane (one lane scenario) receives the packet successfully is $(E(h_i) = E(h) = 1)$:

$$\begin{aligned} P_s &= P\left(\frac{S_1}{I} > \beta\right) \\ &= P\left(\frac{hr^{-\alpha}}{\sum_{i=-\infty}^{\infty} b_i h_i r_i^{-\alpha}} > \beta\right) \\ &= \frac{(1+\beta)}{1+(1-p_{tr})\beta} \cdot \prod_{i=-\infty-\{0\}}^{+\infty} \frac{1+(1-p_i)\beta\left(\frac{m}{i}\right)^{\alpha}}{1+\beta\left(\frac{m}{i}\right)^{\alpha}} \end{aligned} \tag{2.1}$$

where β is the SIR decoding threshold, b_i is a Bernoulli random variable with parameter p_i, node i transmits with probability p_i (the specified transmitter transmits with probability p_{tr}), r_i denotes the distance from the interferer i to the receiver (Fig. 2.2), h_i is the fading coefficient for each time slot (independent slot to slot), and i and m denote the index of interferer i and receiver, respectively. Also, S_1 and I denote the transmitter signal and interference power at the receiver, sequentially. Our assumption is that vehicles (interferers) are located around the receiver to infinity symmetrically. In other words, we are considering the worst case scenario to deal with the highest expected collision probability for our customized approach. We also assume the network is interference limited. Therefore, the nodes can increase their transmit power to overcome the power of noise. The vehicles are not faced with power constraints, hence, this is a realistic assumption for VANETs. Proof:

If there is distance r between a transmitter and the desired receiver, the success probability is

$$
\begin{aligned}
P_s &= P(SIR > \beta) \\
&= P\left(\frac{hr^{-\alpha}}{I} > \beta\right) \\
&= \int P(h > \beta r^{\alpha} I | I = i) f_I(i) di \\
&= \int e^{-\beta r^{\alpha} i} f_I(i) di \\
&= E\left[e^{-\beta r^{\alpha} I}\right] \\
&= E\left[e^{-\beta r^{\alpha} \sum_{i \in \Phi} b_i h_i r_i^{-\alpha}}\right] \\
&= \prod_{i \in \Phi} [E\left[e^{-\beta r^{\alpha} h_i r_i^{-\alpha}}\right] p_i + 1 - p_i] \\
&= \prod_{i \in \Phi} \left[\frac{p_i}{1 + \beta r^{\alpha} r_i^{-\alpha}} + (1 - p_i)\right]
\end{aligned} \tag{2.2}
$$

Assuming,

$$r = mx \quad \text{and} \quad r_i = ix \tag{2.3}$$

Equation 2.1 is obtained.

Theorem:

If the channel access probabilities, $p_i = p$, $\forall i$, are constant, the closed-form packet success probability is ($\alpha = 2$):

$$P_s = \frac{(1+\beta)}{(1-p)[1+(1-p)\beta]} \cdot \frac{\left[\sinh \pi \sqrt{(1-p)\beta} m\right]^2}{\left(\sinh \sqrt{\beta} m\right)^2} \tag{2.4}$$

α is normally in the range of 2 to 4 where 2 is for propagation in free space and 4 is for relatively lossy environments.

Proof:

By plugging Euler's product formula (Equation 2.5) into Equation 2.1, we can obtain Equation 2.4.

$$\sin(\pi z) \equiv \pi z \prod_{i=1}^{\infty} \left(1 - \frac{z^2}{i^2}\right) \tag{2.5}$$

If x denotes the distance between two adjacent nodes, mx represents the distance between receiver and transmitter. It is noteworthy to mention that Equation 2.1 and Equation 2.4 do not depend on the inter-vehicle distance.

There are two approaches for an N-lane highway. The first approach is called the Single Lane Abstraction (SLA) model. In this model, all the traffic lanes are mapped into one lane with the aggregated traffic intensity. Using this model, Equation 2.1 and Equation 2.4 can still be employed to obtain packet success probability. SLA model can be used only if $d^2 \ll mx^2$ in which d shows the distance between two adjacent lanes.

Assume d is the distance between two specific lanes, x denotes the distance between two adjacent vehicles, and the transmitter is located in the middle lane. Let's assume r specifies the distance between transmitter and receiver (which is in a lane with distance d from the middle lane).

$$r = mx\sqrt{1 + \left(\frac{d}{mx}\right)^2} \tag{2.6}$$

$$\approx mx\left(1 + \frac{\left(\frac{d}{mx}\right)^2}{2}\right) \tag{2.7}$$

$$= mx + \frac{d^2}{2mx} \tag{2.8}$$

Therefore, we have shown that if $d^2 \ll mx^2$, $r \approx mx$.

Theorem:

If the inequality does not hold, that approximation cannot characterize the performance of vehicular networks on N-lane highways. If this condition is not satisfied, we cannot ignore d. Therefore, packet success probability can be obtained using:

$$P_s = \frac{(1+\beta)}{1+(1-p_{tr})\beta} \cdot \prod_{i \in -\infty - \{0\}}^{+\infty} \frac{1+(1-p_i)\beta\left(\frac{mx}{ix+\frac{d^2}{2ix}}\right)^2}{1+\beta\left(\frac{mx}{ix+\frac{d^2}{2ix}}\right)^2} \tag{2.9}$$

Proof:

In the proof of Equation 2.1, the last equation is modified with respect to the new assumption that the inter-lane distance cannot be overlooked:

$$P_s = \prod_{i \in \Phi} \left[\frac{p_i}{\left(1+\beta\left(\frac{mx}{ix+\frac{d^2}{2ix}}\right)^{\alpha}\right)} + (1-p_i) \right]$$

Then, Equation 2.9 is obtained.

If the time slots in which nodes transmit are not synchronized, this scheme is named *Slotted Asynchronous P-persistent* (SAP). In this case, an interferer can potentially interfere with *at most* two time slots of another transmission. Hence, the transmission probability for the interferers is:

$$p_i' = p_i + p_i - p_i \cdot p_i \approx 2p_i \tag{2.10}$$

Since the probabilities are small, the approximation is good.

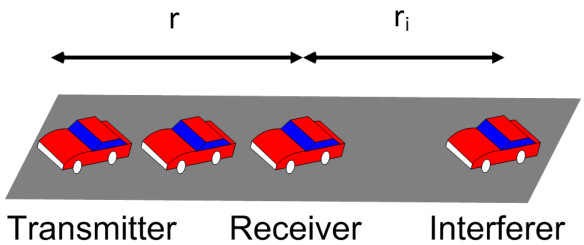

Figure 2.2: A chain of vehicles. Distance between the transmitter and the desired receiver $= r$. Distance between interferer i and desired receiver $= r_i$.

2. Poisson Point Process:

   In this case, the nodes are distributed on a highway according to a Poisson point process (PPP). Poisson point processes have been widely employed as a model for wireless networks [19–21]. The packet success probability can be obtained by considering the fact that the transmitter-receiver distance is a random variable, not a constant value ($E(h) = \lambda = 1$).

$$P_S = P(SIR > \beta) \tag{2.11}$$

$$= \int_r P\left(\frac{P_1 h r^{-\alpha}}{k+I} > \beta\right) f_R(r)dr \tag{2.12}$$

$$= \int_r P\left(h > \frac{\beta(k+I)r^{\alpha}}{P_1}\right) f_R(r)dr \tag{2.13}$$

$$= \int_r e^{\frac{-\beta k r^{\alpha}}{P_1}} \cdot E_I\left[e^{\left(\frac{\beta r^{\alpha}}{P_1}\right)}\right] f_R(r)dr \tag{2.14}$$

$$= \int_r e^{\frac{-\beta k r^{\alpha}}{P_1}} \cdot L_I\left(\frac{\beta r^{\alpha}}{P_1}\right) f_R(r)dr \tag{2.15}$$

if $\quad (k = 0, \alpha = 4, P_1 = 1)$

$$= \int_r L_I\left(\beta r^4\right) f_R(r)dr \tag{2.16}$$

where

- P_1: transmitter signal power
- h: channel fading
- r: distance between transmitter and receiver
- α: path loss exponent
- k: noise variance
- I: interference power
- λ: exponential parameter of Rayleigh fading
- L_I: Laplace transform with respect to I
- E_I: Expectation with respect to I

Assuming the transmitter and receiver are located in the same lane, the distribution of the distance between transmitter and receiver is Erlang:

$$f_R(r) = \frac{\lambda_p^n r^{n-1} e^{-\lambda_p r}}{(n-1)!} \tag{2.17}$$

in which λ_p represents the intensity of vehicles in a lane. Also, n denotes the number of nodes between transmitter and receiver plus one. Elsawy et al. [15] obtains closed-form expressions for the Laplace transform of the aggregate interference. For this specific scenario, this Laplace transform is equal to:

$$L_I\left(\beta r^4\right) = e^{-\pi\lambda_M\left[b^2(1-e^{-\lambda_p\beta K(\frac{r}{b})^4})+(\lambda_p\beta r^4 K)^{\frac{1}{2}}\Gamma(0.5,0.5Kb^{-4})\right]} \tag{2.18}$$

in which

$$\Gamma(s,x) = \int_x^\infty t^{s-1}\cdot e^{-t}dt \tag{2.19}$$

$$K = \left(\frac{c}{4\pi f_c}\right)^2 \tag{2.20}$$

Also, b, c, f_c represent the desired radius from the receiver node in which the aggregate interference is considered, the speed of radio propagation, and the carrier frequency.

Let's assume $\Phi = \{x_i; i = 1, 2, 3, \cdots\}$ are the nodes in the network. Now, we employ the concept of marked point processes [58] since we want to include additional information about the points in the model. A marked point is selected to be retained if and only if it has the lowest mark in a circle of radius L centered at x_i (HCPP-II model). L denotes the minimum distance between any two simultaneously active transmitters. If we assume that the distribution of the marks in one circle is uniform, then the probability of retaining a random point can be written as:

$$P_1 = \sum_{n=1}^{\infty} \frac{1}{n+1} P(\text{having n points in the lane}) \tag{2.21}$$

$$= \sum_{n=1}^{\infty} \frac{1}{n+1} \frac{(\lambda_p L)^n e^{-\lambda_p L}}{n!} \tag{2.22}$$

$$= \frac{1 - e^{-\lambda_p L}}{\lambda_p L} \tag{2.23}$$

λ_M denotes the intensity of the simultaneously active nodes from the parent PPP which is equal to:

$$\lambda_M = P_1 \cdot \lambda_p = \frac{1 - e^{-\lambda_p L}}{L} \tag{2.24}$$

It is often useful to include additional information about the points in the model. Thus, in marked point processes each point x_i is assigned a random variable, the mark m_i. It is necessary to choose m_i in a smart way in order to model the spatial distribution of the active set of interferers. We define m_i as the safety index of vehicle i which means the lowest mark represents the most unsafe vehicle.

Also, see Chapter 5 for additional information on an extension to the HCPP-II model.

2.2.3 Indexing

A number of general indices of driver safety have been suggested or developed with the advent of relatively inexpensive in-vehicle sensors that can record, among other things velocity, acceleration, and lane position. We need to make it clear at the outset that we do not expect to have access to information on the age of a driver or any other demographic information. We assume that the less safe a driver is, the more frequently the driver needs to transmit information to the network. Moreover, the driver safety index could be changed in real time. As an example, if a driver's brake reaction time is relatively long, the driver's safety index will be relatively low, so more data will be put on the air from the corresponding vehicle. In this chapter, vehicles are simply divided into two categories: 1. unsafe vehicles, 2. safe vehicles. Unsafe vehicles are the ones in which their drivers have long PRT and low distance to the vehicle in front (Fig. 2.3). To put it differently, unsafe vehicles have higher collision probability.

Providing the unsafe drivers with more access to the channel actually makes other vehicles safer. In other words, the unsafe vehicles should transmit more frequently to other vehicles. Since these messages help other vehicles avoid collisions, this design awards every vehicle with additional crash avoidance probabilities.

Despite neither disclosing any private information to other vehicles nor imposing a burdensome overhead, sharing safety indices with other vehicles will be of vital importance in improving the safety of the network.

2.3 Customizing Channel Access Probabilities

This section proposes a new algorithm to individualize vehicular communications. Algorithm 1 is a recursive algorithm which adapts channel access probabilities of all

vehicles to the safety needs of drivers in the network. From a safety point of view, three factors are of vital importance for a vehicle: 1. the PRT of the driver, 2. traffic conditions, and 3. communications delay.

Algorithm 1 Algorithm for Customizing Channel Access Probabilities in VANET

Input: Vehicles: $V_1, V_2, \cdots, V_N$, VANET data
Output: Customized channel access probabilities for all vehicles

```
Derive all physical parameters from VANET
(Distances between vehicles, deceleration rates, and velocities)
Divide vehicles into safe and unsafe categories (compute collision probabilities).
Compute the channel access probabilities.
for i = 1 to N do
    Estimate the response time distribution (τ_i).
end for
for i = 1 to N do
    Determine if any type of collision can happen to vehicle i based on both equa-
    tions of motion and the delay of receiving packets from other vehicles.
    if yes then
        p_i = p^u(channel access probability for unsafe vehicles)
    else
        p_i = p^s(channel access probability for safe vehicles)
    end if
end for
return p_{1:N}
```

In one iteration of Algorithm 1, these factors play roles in assigning channel access probabilities to vehicles while the probabilities are being used in the next iteration to compute the new delay of reception at vehicle V_i. Algorithm 1 is of polynomial time. The most time-consuming part of the algorithm is the response time estimation. As we proposed in Chapter 1, the whole estimation computation has complexity $O(n_d^3)$ in which n_d is the number of observations for driver d. we can use the approximated p^s and p^u for a sufficient number of iterations in the algorithm. When new vehicles arrive in the transmission range, those are labeled as safe until the algorithm verifies whether they are causing any peril to other vehicles. Let's assume there are N vehicles on a highway and S vehicles among them are recognized as safe vehicles. A vehicle identifies itself as safe with the probability $\frac{S}{N}$. Clearly, this ratio can vary from time

Table 2.1: Four classes of vehicular communications

Transmitter	Receiver	Percentage of the class
Safe	Safe	$\alpha_1 = \frac{S(S-1)}{N(N-1)}$
Safe	Unsafe	$\alpha_2 = \frac{2S\times(N-S)}{N(N-1)}$
Unsafe	Safe	$\alpha_3 = \frac{2S\times(N-S)}{N(N-1)}$
Unsafe	Unsafe	$\alpha_4 = \frac{(N-S)(N-S-1)}{N(N-1)}$

to time. Furthermore, after a while, any vehicle can move from one category to the other one.

The design goal is to choose p_is such that a sufficiently large P_s is guaranteed for the vehicles and as a result the expected collision probability is minimized. Four classes of communications can be established between any two vehicles (Table 2.1). Thus, packet success probability for the network is stated in the following equation:

$$P_s = \alpha_1 P_1 + \alpha_2 P_2 + \alpha_3 P_3 + \alpha_4 P_4 \tag{2.25}$$

P_i denotes the packet success probability for class i of communication and is obtained by substituting $p_i = p^s$ for any safe vehicle interfering the communication, and $p_i = p^u$ for any unsafe vehicle into a packet success probability equation (e.g. Equation 2.1).

For the PPP scenario, the marks represent the safety index of drivers. The vehicles are sorted based on their safety index and S of them are labeled as safe vehicles. If an unsafe vehicle exists in the disk of another unsafe vehicle, a lower mark will be assigned to the more unsafe vehicle.

Now, we try to find the appropriate value for p^s and p^u by employing the communication and traffic data. Using the first-order Taylor approximation, taking derivative leads us to two quadratic equations. The intersection point of the two ellipsis, described by the following equations, in range [0,1] shows the desired values.

$$
\begin{aligned}
&(p^s)^2\left(-\alpha_1 C_{N-S} B_{S-2} D_{S-2}\right)\\
&+ p^s\left(\alpha_1 C_{N-S} B_{S-2}(D_{S-2}-2) + \alpha_2 C_{N-S-1} B_{S-1} D_{S-1}\right)\\
&+ (p^u)^2\left(-\alpha_4 C_{N-S-2} B_S D_S\right)\\
&+ p^u\left(\alpha_2 C_{N-S-1} B_{S-1}(D_{S-1}-2) + \alpha_4 C_{N-S-2} B_S D_S\right)\\
&+ p^s p^u\left(-2\alpha_2 C_{N-S-1} B_{S-1} D_{S-1}\right)\\
&+ \left(\alpha_1 C_{N-S} B_{S-2} + \alpha_2 C_{N-S-1} B_{S-1}\right) = 0
\end{aligned}
\tag{2.26}
$$

$$
\begin{aligned}
&(p^s)^2\left(-\alpha_1 B_{S-2} C_{N-S} D_{N-S}\right)\\
&+ p^s(\alpha_1 B_{S-2} C_{N-S} D_{N-S}\\
&+ \alpha_2 B_{S-1} C_{N-S-1}(D_{N-S-1}-2))\\
&+ (p^u)^2(-\alpha_4 B_S C_{N-S-2} D_{N-S-2})\\
&+ p^u(\alpha_2 B_{S-1} C_{N-S-1} D_{N-S-1}\\
&+ \alpha_4 B_S C_{N-S-2}(D_{N-S-2}-2))\\
&+ p^s p^u(-2\alpha_2 B_{S-1} C_{N-S-1} D_{N-S-1})\\
&+ (\alpha_2 B_{S-1} C_{N-S-1} + \alpha_4 B_S C_{N-S-2}) = 0
\end{aligned}
\tag{2.27}
$$

in which

$$
B_S^{(j)} = \prod_{i=1}^{S}\left[\frac{(p^s)^{(j-1)}}{1+\beta r^\alpha r_i^{-\alpha}} + (1-(p^s)^{(j-1)})\right] \tag{2.28}
$$

$$
C_{N-S}^{(j)} = \prod_{i=1}^{N-S}\left[\frac{(p^u)^{(j-1)}}{1+\beta r^\alpha r_i^{-\alpha}} + (1-(p^u)^{(j-1)})\right] \tag{2.29}
$$

$$
D_S = \sum_{i=1}^{S}\left[\frac{1}{1+\beta r^\alpha r_i^{-\alpha}}\right] - S \tag{2.30}
$$

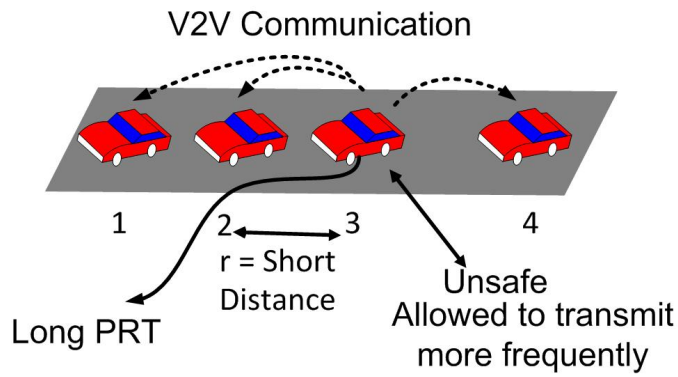

Figure 2.3: Vehicle 3 needs to transmit more frequently than other vehicles because it has higher collision probability.

The coefficients have to be computed carefully since it is important to know which vehicles are included in the multiplications. After B_S, C_{N-S}, and D_S are obtained in each iteration (j is the iteration number - the intial values of the channel access are 0.02), p^s and p^u will be computed in the next one. Our Monte Carlo simulation results show that, on average, the optimized probabilities found by brute-force search algorithm results in the expected collision probability that is only $< 1\%$ less than that obtained from employing the optimized values of the channel access. This means the approximated values are sufficiently close to the real values.

2.4 Numerical and Simulation Evaluation of Design

When vehicular communications are employed, communications delay is a main factor that influences the vehicle collision probability on highways. Also, we know that some of the vehicles are too far from the vehicle V_0 (the leading vehicle) to be able to receive the messages directly from it. Thus, when one of the vehicles in the middle gets informed and reacts to the event, the message will be forwarded to the vehicles at a greater distance from the leading vehicle. In other words, after a vehicle in the middle starts decelerating, the new status will be included in the new messages from this vehicle to further upstream vehicles. Therefore, we need to

compute the time it takes for a message to be received by vehicle i. It is sufficient that the message be received successfully only one time. The delivery of safety packets is not generally independent time slot to time slot for the PPP model. However, in our simulations, in order to calculate the collision probability in a network, we assume p^s and p^u change only after the packet is received by the desired receiver (not in each time slot). Therefore, delivery of the packets can be considered as nearly independent events. Therefore, when this assumption holds, $P_s(i)$ is given by Equation 2.16. Fig. 2.5 shows if Algorithm 1 is employed in each time slot, the independency approximation is good only when the traffic is light (PPP is an efficient model to describe the light traffic). Also, Equation 3.8 is employed in order to plot the non-independent curves. For the equal distance scenario, the successful reception at vehicle V_i has a geometric distribution with parameter

$$P_s(i) \cdot p_{tr} \cdot (1 - p_i) \tag{2.31}$$

where $P_s(i)$ is given in Equation 2.1, Equation 2.4, and Equation 2.9. Also, p_{tr} and p_i represent the channel access probability for the transmitter and the desired receiver (i^{th} vehicle) respectively.

This gives us the number of required slots on average for vehicle V_i to receive vehicle V_0's messages:

$$s(i) = \frac{1}{P_s(i) \cdot p_{tr} \cdot (1 - p_i)} \tag{2.32}$$

If SAP scheme is employed, we need to alter the equation:

$$s(i) = \frac{1}{P'_s(i) \cdot p_{tr} \cdot (1 - p'_i)} \tag{2.33}$$

in which p'_i represents the channel access probability when the time slots are not synchronized and $P'_s(i)$ denotes Equation 2.1 using the new channel access probabilities.

Table 2.2: Collision scenarios between V_0 and V_1 in a chain of vehicles. V_1 follows V_0 in the chain. For example, collision type 1 happens when the leading vehicle V_0 is decelerating and the driver of the following vehicle has not perceived the incident yet.

Collision 1	Collision 2
Before V_0 stops Before V_1 Reacts	After V_0 stops Before V_1 Reacts
Collision 3	Collision 4
Before V_0 stops After V_1 Reacts	After V_0 stops After V_1 Reacts

The allowable number of transmission opportunities within the tolerable delay period is:

$$D = \lfloor \frac{T(i)R}{L_p} \rfloor \tag{2.34}$$

where R represents the data rate which is chosen from Table 2.3 while L_p denotes the packet length. $T(i)$ denotes the maximum tolerable delay to inform vehicle V_i which can be obtained from Fig. 2.4 and Table 2.2. Fig. 2.4 shows the time left for the driver of the following vehicle to react to the braking of the leading vehicle enforced by the mobility equations in a dense traffic. Different types of collisions are described in Table 2.2. Vehicle V_0 represents the leading vehicle in a chain while vehicle V_1 is the follower. Based on the amount of time available for the driver of V_1 to apply the brake, the collision may happen when each of these two vehicles have different status. Let P_s^D denote the success probability at V_j after D transmission opportunities:

$$P_s^D = 1 - (1 - s(j)^{-1})^D$$

This equation demonstrates the dependence of packet success probability on channel access probabilities and inter-vehicle distances. Fig. 2.5 illustrates the success

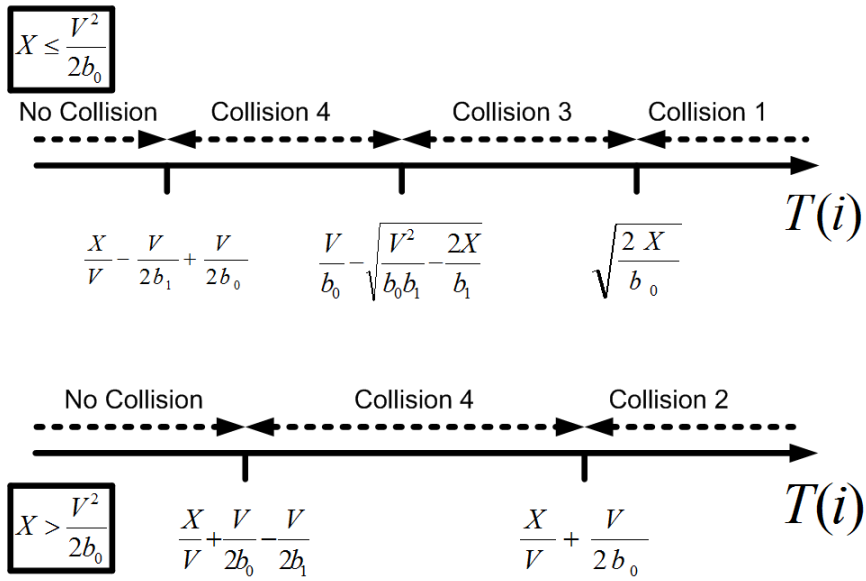

Figure 2.4: An example of collision scenarios between vehicles V_0 and V_1 in dense traffic. V_1 follows V_0 in a chain of vehicles. X, V, and b represent inter-vehicle spacing, velocity, and deceleration rate respectively.

Table 2.3: IEEE 802.11P data rates and corresponding SIR decoding thresholds

R (Mbps)	3	4.5	6	9	12	18	24
β (db)	5	6	8	11	15	20	25

probability after D transmissions by employing the obtained equations for different expected inter-vehicle distance. Clearly, it takes longer time for the vehicles far away from V_0 to receive the packets due to delay. However, those far vehicles (for example V_j) receive the messages about the deceleration of V_0 from the vehicles $V_1 \cdots V_{j-2}$ as well. V_{j-1} is not included since V_j can see the brake lights of V_{j-1} with no need of vehicle-to-vehicle communications. Taking all of the above into account, the average delay of reception at vehicle V_i is:

$$D(i) = min(min_{(j \in 1,\cdots,i-2)} \frac{L_p}{R} s(j) + \tau_j + \frac{L_p}{R} s(i-j), \frac{L_p}{R} s(i), \frac{L_p}{R} s(i-1) + \tau_{i-1}), \quad i > 2 \tag{2.35}$$

Table 2.4: Simulation parameters in a specific part of the highway. Data rate and SIR decoding threshold are chosen based on [17]

Distribution	Poisson Equal distance
Velocity	$30\frac{m}{s}$
Deceleration rate	$[-4, -8]\frac{m}{s^2}$
Total number of vehicles	32
Total number of unsafe vehicles	4
SIR decoding threshold	11 dB
Data rate	9 Mbps
Packet length	250 Bytes
Poisson average	$\frac{1}{25m}$

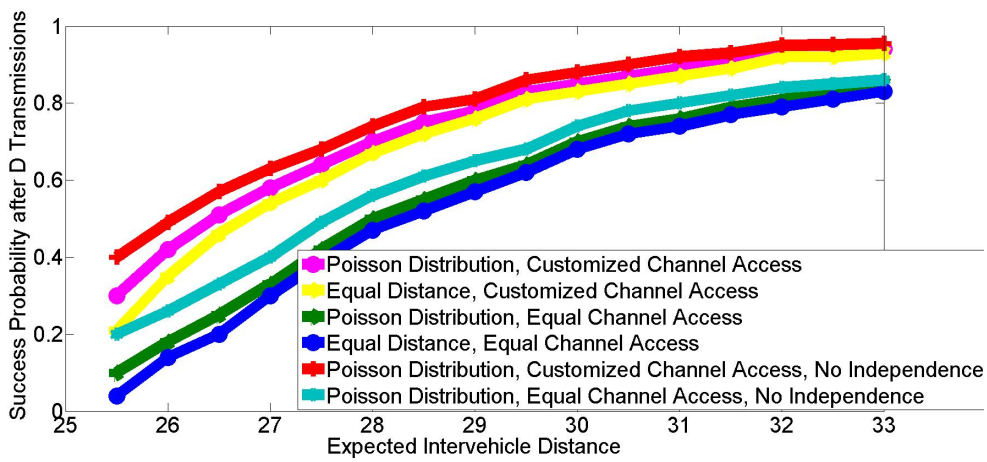

Figure 2.5: Packet success probability after D transmissions at vehicle V_2 for different traffic models and different expected inter-vehicle distance(meters).

where $s(1) = D(1) = 0$ since there is no need for communications between two adjacent vehicles. Also, for each retransmission of a safety packet, the PRT value of the middle vehicle is added to the communication delays. Therefore, communicating from the transmitter to the receiver by using more than two other vehicles always takes longer time than one hop and two hop communications. If the distance between a vehicle and the one ahead of it is short, and also the PRT of the following vehicle is long enough, we consider the vehicle unsafe. Otherwise, the vehicle is a safe one.

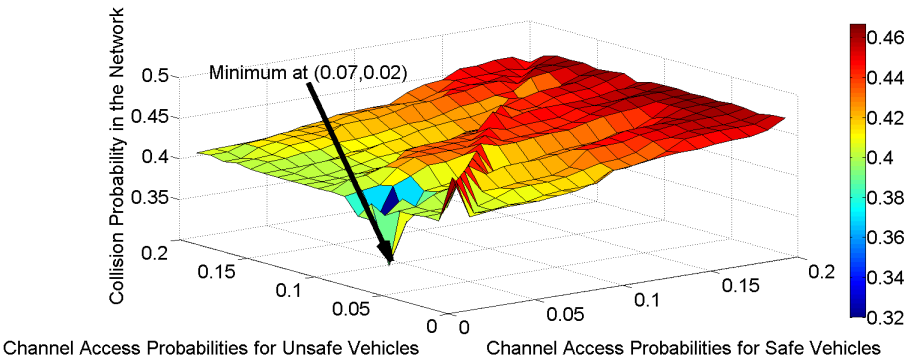

Figure 2.6: The X, Y, and Z axes represent channel access probability for safe vehicles, channel access probability for unsafe vehicles, and collision probability average over all vehicles respectively. Vehicles' locations are randomly drawn from the Poisson distribution. The minimum collision probability in this case is 25% less than the scenario in which equal channel access probabilities are assigned to all vehicles. Therefore, we conclude that tailoring the channel access probabilities to unsafe and safe vehicles leads the network to reduction of collision probability.

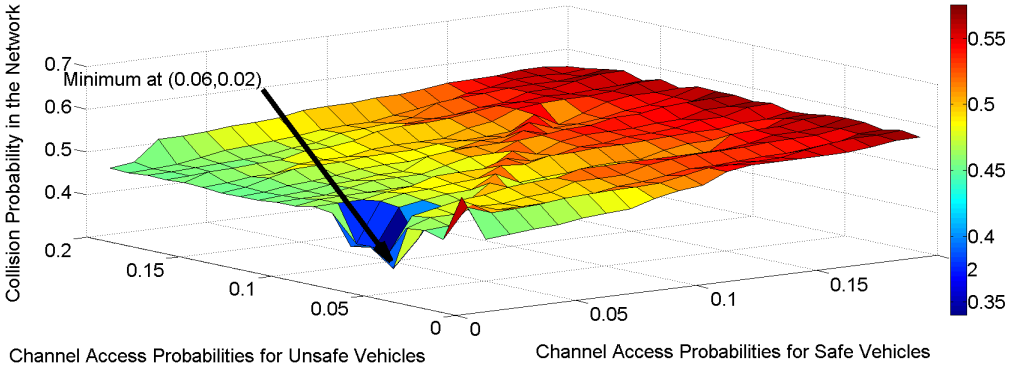

Figure 2.7: Vehicle collision probability versus channel access probability for safe and unsafe vehicles. The inter-vehicle distance is assumed to be equal for all vehicles.

In other words, if the collision probability calculated based on only physical/traffic parameters (without considering the vehicle-to-vehicle communication) is higher than a threshold, the vehicle is unsafe. We can run algorithm 1 recursively such that the

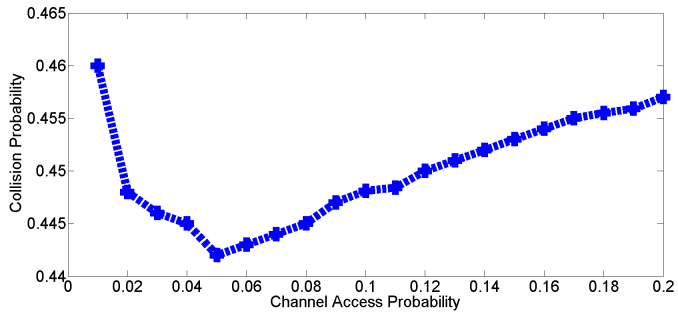

Figure 2.8: Collision probability versus channel access probability. Channel access probability is assumed to be equal for all vehicles. Vehicles' locations values are generated from Poisson distribution.

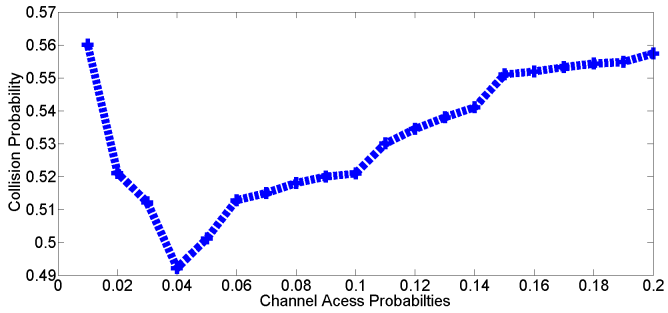

Figure 2.9: Collision probability versus channel access probability. Channel access probability is assumed to be equal for all vehicles. Also, the vehicles' distances are assumed to be equal.

channel access probability at a specific time depends on the collision probability at the previous time.

We run Monte Carlo simulations to study vehicle collisions within a chain. The simulation was carried out as follows. First, the vehicles are placed in a lane (with the number generated from a Poisson distribution with the average shown in Table 2.4 for the PPP scenario). Next, a chain consisting of 32 vehicles were chosen and 4 of them were considered as unsafe. Each vehicle was assigned p^s if it was safe and p^u if it was unsafe. We consider the perception reaction time of drivers being independently drawn from a log-normal distribution with parameters 1.31 and 0.61 [39]. Moreover, we assume that each vehicle can decelerate with a rate chosen uniformly at random

from the interval $[-8-4]\frac{m}{s^2}$. All the vehicles are moving in the same direction while the first vehicle in the chain start decelerating and communicating to other vehicles. The packet success probabilities are obtained by employing Equation 2.16 and Equation 2.1. Next, different types of collisions for any two adjacent vehicles are defined based on Table 2.2. Therefore, we can obtain the collision probability of vehicles in the chain by employing the motion equations of vehicles (Fig. 2.4) and repeating the experiment for 1000 iterations. Algorithm 1 is run after each successful packet delivery with the parameters shown in Table 2.4 to obtain the new channel access for the next time slot.

In our model, the drivers can only avoid accidents by applying the brake. Furthermore, most of the drivers tend to keep a minimum distance with the lead vehicle which is ignored in our model because that is not always the case. In other words, we actually calculate an upper bound for the collision probability which shows us to a great extent how this probability really varies for the scenarios which lead to deadly collisions.

Using simulation parameters in Table 2.4, Fig. 2.6 illustrates the collision probabilities when different channel access probabilities are assigned to unsafe and safe vehicles. Obtained collision probability values are greater than what we usually expect based on our life experience since these probabilities are computed conditional on the scenarios in which a high number of collisions is expected (e.g. no maximum for the PRTs and no minimum for the distance between vehicles are considered). This is what we intend to do because these scenarios usually result in more deadly collisions. Therefore, we aim at reducing the deadly collisions rather than the non-deadly ones.

In Fig. 2.6, X axis represents the channel access probabilities for safe vehicles, Y axis shows the channel access probabilities for unsafe vehicles, and Z axis denotes the collision probabilities. Assuming equal transmission probabilities (Fig. 2.8), the minimum number of collisions happens at around $p_0 \approx 0.05$. However, 25% reduction

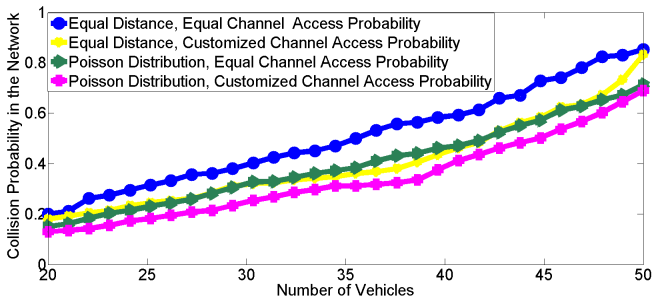

Figure 2.10: Collision probability in the chain versus the number of vehicles. The length of the specified part of highway is assumed to be 500 meters. The other parameters are chosen from Table 2.4. The comparison is between four cases (Vehicle locations, Communications): 1. Equal distance, equal channel access probability. 2. Equal distance, customized channel access probability. 3. Poisson distribution, equal channel access probability. 4. Poisson distribution, customized channel access probability.

in collision probability can be achieved when unsafe and safe vehicles transmit with specific probabilities more and less than p_0 respectively. In other words, the minimum collision probability in Fig. 2.6 is located in a value greater than p_0 on Y axis and less than p_0 on X axis. Here, we are actually comparing these customized communications (Fig. 2.6) to the communications with equal channel access probabilities in its optimized range (Fig. 2.8). With this simulation, it becomes clear that using the driver-based adaptation of communications in warning systems has a noticeable advantage over these systems employing the most appropriate equal channel access probabilities for all vehicles and therefore has a huge advantage over the currently used warning systems. Similarly, Fig. 2.7 illustrates how the number of collisions is reduced when the customized design is employed compared to Fig. 2.9.

Fig. 2.10 illustrates the advantage of employing the customized communications in a 500-meter part of a highway, assuming a different number of vehicles are placed on that part. The simulation is conducted as follows. The vehicles are placed in a lane based on either Poisson distribution or equal distance scenario. They all move in the same direction. We look at the vehicles in the 500 meters part of a highway in

order to calculate the collision probabilities. By employing Table 2.2 and Table 2.4, Fig. 2.10 is obtained.

If we use the same simulation parameters for the equal-distance scenario, even greater reduction in collision probabilities are achieved. This seems to be justifiable because the equal-distance model represents the dense traffic, thus more collisions happen.

2.5 Conclusion

So far, we've shown not only how we can estimate individual driver's characteristics from vehicular ad hoc networks data, but also how we can use that estimate to optimize the communications among vehicles of critical crash relevant information. Drivers characterized as safe will place less of a burden on the communications network because information from these drivers can be transmitted less often than is information from drivers who are characterized as unsafe. Thus, by taking into account the traffic and drivers' characteristics one can potentially improve the delivery of timely warning messages to drivers while substantially reducing the collision probability. Our research suggests that using this strategy the functioning of the rear-end collision warning systems can be dramatically improved as compared to similar systems which do not account for both the specifics of particular drivers and traffic.

CHAPTER 3

THE EFFECT OF COMMUNICATION INTERFERENCE ON SAFETY FACTORS IN A VANET

In Chapter 2, we proposed an algorithm to customize the vehicular communications to the drivers' needs. We know the communication interference affects the drivers' safety noticeably. Rayleigh fading model was employed in Chapter 2, however, a number of other models exist to describe the statistics of the amplitude and the phase of multi-path fading signals. The Nakagami-m distribution has some advantages over other models like Rayleigh fading and Rician fading. However, many papers have considered the simpler models to analyze the interference at the expense of losing the required accuracy. Carrier sensing has also been a neglected factor in the safety packets' delivery analysis. Our main contributions in this chapter are as follows:

- We analytically study the delivery rate of safety packets by taking the multi-user interference, path loss, and two different types of fading models into account.
- We also consider the scheme in which each node senses the channel at the beginning of each slot.
- We compare the packet success probability and vehicle collision probability for each discussed scheme.

Our goal is to examine how many transmissions on average are required for a vehicle in order to receive the desired safety packet. There are major differences between our work and others'. First, most of the studies which examine different

interference models are only simulation-based (e.g. [74] and [75]). However, we want to find insights on how different parameters can actually change the delivery of packets and thus the vehicle collision probability. Clearly, the results obtained from both different simulators and analysis are only an approximation of reality. Second, we will demonstrate the effect of carrier sensing (or non-independent channel access of vehicles) on the packet success probability which is usually neglected in the analysis. Third, the channel access is assumed to be equal for different vehicles in the analysis. Although this assumption seems realistic based on the current vehicles equipped with DSRC antennas, in the near future this assumption may need to be relaxed. In other words, as was discussed in Chapter 2, the channel access of different drivers will depend on the safety of their vehicles in future designs. Hence, we assume the vehicles can transmit at different rates.

3.1 Analysis

We need to know the communication interference of other vehicles' signals in order to find any other important safety factors in our design, factors such as packet delivery success probability and vehicle collision probability.

Path loss and Nakagami-m fading are taken into account for formalizing the signal propagation characteristics. If the nodes transmit with unit power, the received power at distance r is $hr^{-\alpha}$ where $\alpha(> 1)$ is the path loss exponent and h is the fading coefficient. We assume that the magnitude of the signal that has passed through the transmission medium will vary randomly according to the Nakagami-m distribution. This is a valid assumption because the sum of multiple independent and identically distributed (i.i.d.) Rayleigh-fading signals, which have a Nakagami distributed signal amplitude, have been shown to be an efficient interference model for multiple sources [55]. Since the amplitude of the received signal is a Nakagami-m distributed random variable, h has gamma distribution with mean λ:

$$f_H(h) = \frac{1}{\Gamma(m)} \left(\frac{m}{\lambda}\right)^m h^{m-1} e^{\frac{-mh}{\lambda}} \quad h \geq 0$$

where $\Gamma(m)$ is the gamma function for integer shape factor m. Assuming that a vehicle transmits a packet, the per-hop transmission success probability can be calculated as follows ($E(h_i) = \lambda = 1$):

$$P_S = \mathbb{P}\left(\frac{S}{I} > \beta\right) \tag{3.1}$$

$$\begin{aligned} P_S &= \mathbb{P}\left(\frac{hr^{-\alpha}}{\sum_{i=1}^{n} b_i h_i r_i^{-\alpha}} > \beta\right) \\ &= \int \mathbb{P}\left(h > \beta r^{\alpha} I | I = i\right) f_I(i) di \\ &= E_I\left[1 - \frac{1}{\Gamma(m)} \gamma(m, m\beta r^{\alpha} I)\right] \\ \gamma\left(m, m\beta r^{\alpha} I\right) &= \frac{1}{\Gamma(m)} \sum_{k=0}^{\infty} \frac{(-m\beta r^{\alpha} I)^k}{k!(m+k)} \end{aligned} \tag{3.2}$$

$$P_S = 1 - \frac{1}{\Gamma(m)} m^m \sum_{k=0}^{\infty} \frac{(-m)^k \beta^{k+m}}{k!(k+m)} E[r^{\alpha} I]^{(k+m)} \tag{3.3}$$

$$= 1 - \frac{1}{\Gamma(m)} \sum_{k=0}^{\infty} \frac{(-1)^k \beta^k}{k!(m+k)[(m-1)!]^k} \cdot \prod_{i=1}^{n} p_i$$

$$\cdot \sum_{k_1+k_2+\cdots+k_n=k} \begin{pmatrix} k \\ k_1, k_2, \cdots, k_n \end{pmatrix} (m + k_i - 1)! \cdot E\left[\left(\prod_{j=1}^{n} \left(\frac{r}{r_j}\right)^{\alpha k_i}\right)\right] \tag{3.4}$$

$$\begin{pmatrix} k \\ k_1, k_2, \cdots, k_n \end{pmatrix} = \frac{k!}{k_1! \cdot k_2! \cdots k_n!}$$

The definitions of the variables are given in Table 3.1. A fixed coding scheme is

Table 3.1: Definitions of the variables in Equation 3.1, Equation 3.2, Equation 3.3, Equation 3.4

S	Desired signal power
I	Interference power at the receiver
α	Path loss exponent
β	SIR decoding threshold
p_i	Transmission probability of node i
b_i	Bernoulli random variable with probability p_i
r_i	Distance from the interferer i to the receiver
r	Distance between the transmitter and the receiver
n	Number of vehicles
h_i	Fading coefficient of interferer i

considered in Equation 3.1 that requires the SIR at the receiver to be greater than some threshold which is chosen based on IEEE 802.11p tables [3] (e.g. Table 2.3). S denotes the power of the main signal which faces interference from the other vehicles with the accumulative power of I. Equation 3.2 is then obtained by substituting the definitions of the transmitter signal strength and the interference signal strength in Equation 3.1. Each of the vehicles is either in the transmitting mode with probability p_i or in the receiving mode with probability $1 - p_i$. A Bernoulli random variable, b_i, represents this state of vehicle i. Equation 3.3 is resulted by employing the following convergent series of the incomplete gamma function to cancel h.

$$\gamma\left(m, m\beta r^{\alpha} I\right) = \frac{1}{\Gamma(m)} \sum_{k=0}^{\infty} \frac{\left(-m\beta r^{\alpha} I\right)^{k}}{k!(m+k)}$$

Finally, the multinomial expansion and characteristic functions of fading random variables leads us to Equation 3.4.

The obtained packet success probability equation clearly holds while there is no constraint on any specific geometry. For $m = 1$, Equation 3.3 will be equal to:

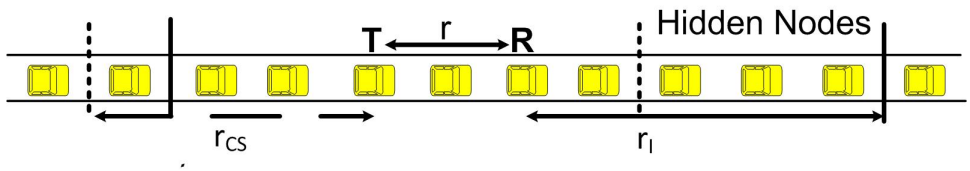

Figure 3.1: A chain of vehicles which employs SAP/CS MAC scheme.

$$P_S = \prod_{i=1}^{n} \left[1 - p_i + \frac{p_i}{1 + \beta \left(\frac{r}{r_i} \right)^{\alpha}} \right] \tag{3.5}$$

which is the packet success probability equation when the Rayleigh fading model is employed [77].

Up to this point, we have assumed that each vehicle transmits independent of all other vehicles. However, in order to reduce the probability of packet collisions, we study a channel sensing scheme in which each vehicle transmits only if it finds the channel idle. Our goal is to find the packet success probability under the Nakagami-m fading model by employing the SAP/CS scheme. To make the analysis feasible, we start with:

$$P_s = P_t \cdot P_{s|t}$$

P_t represents the probability that node T accesses the channel, i.e. finds it idle and transmits. $P_{s|t}$ is the packet success probability at vehicle R, given that vehicle T accesses the channel. We define the carrier sensing distance as r_{CS}. A vehicle can

transmit if and only if no other vehicle transmits within r_{CS} distance of it. The number of vehicles within this radius is called n_{CS}:

$$P_t \approx p_T \prod_{i=1}^{n_{CS}} (1 - p_i) \tag{3.6}$$

in which p_T represents the channel access probability of the transmitter vehicle. The right-hand side of the Equation 3.6 is sufficiently close to the left-hand side because transmission probabilities are small (despite the transmissions not being independent). If the probabilities are not small, Equation 3.6 denotes a lowerbound for P_t.

Next, in order to find the packet success probability, we need to find the radius of a disk centered at R in which any active node can cause interference at R. According to the SIR-based reception model, there must be $\frac{hr^{-\alpha}}{h_i r_i^{-\alpha}} > \beta$ where h and h_i are the respective Nakagami-m fading components of the interference model, and r and r_i are the distance between the transmitter and the receiver and the distance between the interferer i and the receiver. Therefore, we have:

$$r_I \approx r\beta^{\frac{1}{\alpha}} \mathbb{E}\left[h^{\frac{-1}{\alpha}}\right] \mathbb{E}\left[h_i^{\frac{1}{\alpha}}\right]$$

By employing the concept of fractional moments, we obtain:

$$r_I \approx r \cdot \beta^{\frac{1}{\alpha}} \frac{\Gamma(m + \frac{1}{\alpha})}{\Gamma(m)} \frac{\Gamma(m - \frac{1}{\alpha})}{\Gamma(m)}$$

$$= r \cdot \beta^{\frac{1}{\alpha}} \frac{\frac{\pi}{\alpha}}{\Gamma^2(m)} \csc(\frac{\pi}{\alpha})$$

For the Rayleigh fading scenario ($m = 1$),

$$r_I \approx r \cdot \beta^{\frac{1}{\alpha}} \frac{\pi}{\alpha} \csc(\frac{\pi}{\alpha})$$

In the absence of fading, $r_I \approx r\beta^{\frac{1}{\alpha}}$. When vehicle T transmits, only the hidden nodes whose activities are not sensed by node T can cause outage at node R (see Fig. 3.1). If there are x hidden nodes and N_i represents the event that the ith hidden node does not transmit, then $P_{s|t}$ is equal to

$$P_{s|t} = \mathbb{P}\left(\bigcap_{i=1}^{x} N_i\right) = 1 - \sum_{i=1}^{x} \mathbb{P}(N_i^c) \tag{3.7}$$

The last equality is true when $N_i^c \bigcap N_j^c = \emptyset$. This condition holds true since the MAC scheme does not allow the hidden nodes to transmit simultaneously for the practical values of r_{CS} and r_I. For a one lane case, the packet success probability of the transmitter T at the receiver R can be approximated as:

$$P_s \approx \begin{cases} p_T \prod_{i=1}^{n_{CS}} (1-p_i) \left[1 - \sum_{i=1}^{N(r+r_I-r_{CS})} p_i^{'}\right] & max\left(r_I - r, \frac{r+r_I}{2}\right) \leq r_{CS} < r + r_I \\ \\ p_T \prod_{i=1}^{n_{CS}} (1-p_i) & r_{CS} \geq r + r_I \end{cases} \tag{3.8}$$

$N(r+r_I-r_{CS})$ represents the number of hidden nodes in the hidden area $(r+r_I-r_{CS})$. The optimized carrier sensing distance is $r_{CS}^* \approx r + r_I$. Here, $r_I - r \leq r_{CS}$ represents the scenario when there is no hidden node on the left side of node T. In order for Equation 3.7 to hold, $\frac{r+r_I}{2}$, which is the maximum distance between the hidden nodes, must be less than r_{CS} to force the vehicles not to be transmitting together.

3.2 Numerical Results

In this section, we want to compare the performance of different models in a highway scenario considering both discussed cases, with and without carrier sensing. Table 3.2 shows all the values assigned to different parameters. In a chain of vehicles, we assume transmissions across the chain are partially obstructed by some vehicles that are chosen uniformly in our Monte Carlo simulations. In other words,

Table 3.2: Simulation Parameters. Data rate and SIR decoding threshold are chosen based on [17]

Vehicle Distribution	Poisson(20)
Velocity	$20\frac{m}{s}$
Deceleration rate	$[-6,-9]\frac{m}{s^2}$
Total number of vehicles	25
SIR decoding threshold	8 dB
R=Data rate	6 Mbps
Number of Obstructive Vehicles	4
L=Packet length	250 Bytes
Reaction times of drivers	$ln\mathbf{N}(0.17, 0.44)$

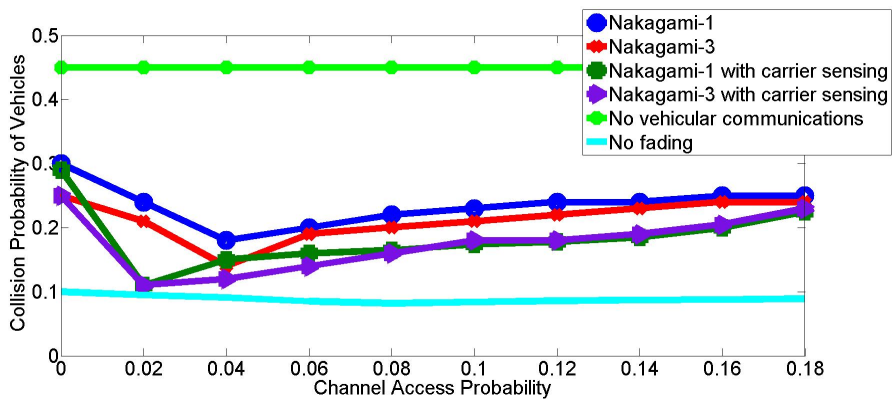

Figure 3.2: The average collision probability of vehicles versus channel access probability. We have employed these equations to plot the figure: Equation 3.5 for Nakagami-1 without carrier sensing, Equation 3.4 for Nakagami-3 without carrier sensing, Equation 3.8 for the carrier sensing design.

the selected vehicles disrupt the line-of-sight environment for the specific scenario and divide the chain into smaller chains. The collision probability is calculated based on the equations of motion. The drivers can react to the deceleration of their leading car with reaction time chosen randomly from the lognormal distribution with parameters $\mu = 0.17$ and $\sigma = 0.44$ (see [39]). The vehicles transmit with equal channel access probability and the distance between vehicles is chosen from the exponential distribution (see [14]) with a mean of 20 meters. Therefore, the packet success probability

is obtained by employing Equations 3.8, 3.5, and 3.4. Also, each vehicle decelerates as soon as it is informed with a rate chosen uniformly at random from the interval $[-6, -9]\frac{m}{s^2}$ (see Table 3.2). The average collision probability of vehicles (conditional on the described scenario) is illustrated in Fig. 3.2. When the channel access probability is small, the communication with carrier sensing is almost the same as the scenario without carrier sensing. Therefore, when the vehicles are sensing the channel, almost the same average collision probability is achieved at smaller channel access than is the case without carrier sensing. Also, for large channel access the difference between the schemes with and without carrier sensing shrinks. There is only a small critical range for which at most around 10% reduction in the collision probability is achieved. Since the Equation 3.6 represents a lowerbound for the success probability, the resulting reduction achieved by employing the carrier sensing is the maximum possible difference between the two curves. Therefore, it confirms that carrier sensing could be relatively efficient only in a specific range. Fig. 3.2 also depicts that employing the more accurate model (Nakagami-3) results in lower collision probability especially when carrier sensing is used.

3.3 Conclusion

In this chapter, we study the effect of Nakagami-m propagation model on the delivery of safety packets in vehicular ad hoc networks. Also, we derived the approximated packet success probability for the scenario which vehicles sense if the channel is idle. Our results illustrate how employing the Nakagami-3 fading for the design of the safety systems leads to lower collision probability compared to Rayleigh fading while carrier sensing is only useful in a small specific range of channel access for different vehicles in a chain.

CHAPTER 4

SIMILAR AD HOC NETWORKS TO VANET: UNMANNED AERIAL VEHICLE NETWORKS

Drones, Unmanned Aerial Vehicles (UAVs), or Unmanned Aircraft Systems (UAS) are all keywords to describe a system of aircrafts without a human pilot on board. While the military usage of UAVs has started long ago, commercial applications of UAVs is an emerging hot topic. Some examples of applications of UAS include providing aerial photos and video at a fraction of the cost of traditional methods that can be used in crop monitoring, construction site management, film-making, fire-fighting, disaster management and avalanche control. Wireless communications are of vital importance in order to improve the efficiency of performing the desired applications. Several challenges such as coverage considerations and spectrum policy are discussed in other publications [66], [67], [68]. The majority of the studies are focused on air-ground communications between a single UAV and multiple ground centers instead of analyzing the possible UAVs ad hoc networks [70], [71]. Building a multi UAV network improves many required aspects of the described applications (see Table 4.1). Constructing ad hoc networks of UAVs requires dealing with tradeoffs which restrict the number of UAVs covering an area. In this chapter, we consider one transportation measure (safety), one application measure (coverage), and two communication measures (interference and connectivity) in order to find the needed range of intensities by considering the specific characteristics of UAVs.

Table 4.1: Comparison between a single UAV system and a multi-UAV network. (Taken from [57])

Feature	Single-UAV system	Multi-UAV system
Scalability	Limited	High
Survivability	Poor	High
Speed of mission	Slow	Fast
Cost	Medium	Low
Bandwidth	High	Medium
Antenna	Omni-directional	Directional

4.1 The Model

In the near future, there will be a large number of UAVs flying over many areas by different public or private organizations as well by individuals. Since these UAVs are operated by many different entities, we assume that the times, the locations, and the directions of their flights are statistically independent. Also, since most of these UAVs fly at about the same altitude, we can model the locations of these UAVs at any time as a homogenous two-dimensional PPP:

$$\Phi = \{x_1, x_2, x_3, \cdots\}.$$

The probability of having n UAVs in a compact set $A \subset \mathbb{R}^2$ is represented by:

$$P(|A \cap \Phi| = n) = \frac{(\lambda \widetilde{A})^n e^{-\lambda \widetilde{A}}}{n!}$$

where $|\cdot|$ denotes set cardinality and $\widetilde{A}$ is the Lebesgue measure of A. In addition, by the displacement theorem ([58] page 35), the locations of the UAVs will constitute a PPP for all the future times (assuming their final destinations are different). The key factor in the above model is the intensity parameter λ. It shows the average number

of the UAVs in the corresponding area. Based on the transportation factors, we can calculate the parameter λ in any time interval for the Poisson process as:

$$\lambda = \frac{\text{Take-off Rate} \times \text{Flight Duration}}{\text{Area of the Region}} \quad \frac{takeoffs}{\text{hectare}}.$$

4.1.1 Safety

The current low intensity of UAVs in the sky means that there is little concern regarding close encounters or collisions of the UAVs. That, however, will change as both the number and thus the intensity of the UAVs increase drastically within the next few years. As the intensity of UAVs in the sky increases, the probability of close encounter between UAVs increases dramatically. Thus, the natural question is what ranges of intensity (λ) are feasible when we want to have a certain level of safety. Therefore, we need to mathematically define a safety measure. For any UAV in the sky, we require that the probability that another UAV is closer than d_s units of distance to the UAV is less than p_s (safety criteria). This is referred to as probability of close-encounter. p_s is not the collision probability; it is however, a measure that is related to collision probability. The collision probability will be a value that is much smaller than p_s. Assuming the Poisson model and the safety criteria, we can write:

$$1 - \exp\left(-\lambda \pi d_s^2\right) < p_s$$

so we obtain:

$$\lambda < \frac{1}{\pi d_s^2} \ln\left(\frac{1}{1 - p_s}\right). \tag{4.1}$$

Equation 4.1 shows that for safe operation, the intensity λ should be kept under the above threshold.

4.1.2 Coverage

In many applications, the UAVs are enabled to monitor a region of interest for purposes such as search and rescue, surveying, and crop monitoring. Let's assume each UAV is capable of covering a region S and the area of S, shown by $|S|$, is generally a random variable. What range of λ does ensure a network of UAVs cover a certain region? If $\mathcal{R}$ is the region of interest and the vacancy, shown by $V(\mathcal{R})$, is defined as the area of the region that is not covered, then, we have ([58] page 255):

$$E(V(\mathcal{R})) = |\mathcal{R}| \exp\left(-\lambda E|S|\right),$$

where $|\cdot|$ shows the area. The coverage condition can be then stated as:

$$E(V(\mathcal{R})) < v_{th}|\mathcal{R}|,$$

where v_{th} is the maximum allowable portion of the area that can be uncovered. Then, we obtain:

$$\lambda > \frac{1}{E|S|} \ln\left(\frac{1}{v_{th}}\right). \tag{4.2}$$

Thus, to ensure the assumed coverage requirement, the intensity of the drones in the region must be larger than the above threshold. Combining Equation 4.1 and Equation 4.2, we conclude that the appropriate value for the intensity of drones must be in the following range:

$$\frac{1}{E|S|} \ln\left(\frac{1}{v_{th}}\right) < \lambda < \frac{1}{\pi d_s^2} \ln\left(\frac{1}{1-p_s}\right). \tag{4.3}$$

4.1.3 Interference

4.1.3.1 No Carrier Sensing

Wireless communications can be an important tool in a UAS. UAVs should be able to communicate wirelessly to receive and transmit data from both the ground and other UAVs to ensure appropriate and safe operation. An important requirement in UASs is that the resulting interference should be kept under some threshold. Here, we study this question for the above Poisson-based model. A common model for path loss function is:

$$\ell(x) = \min\{1, \|x\|^{-\alpha}\}$$

where α is called the path loss exponent. Let's assume $\alpha > 2$. Then, our goal is to compute the mean interference EI at each UAV when a portion a_I of the UAVs are transmitting. This problem can be solved with Campbell's formula ([58] page 83):

$$\begin{aligned} EI &= a_I \lambda \int_{\mathbb{R}^2} \min\{1, \|x\|^{-\alpha}\} dx \\ &= \lambda a_I \int_0^{2\pi} \int_0^{\infty} \min\{1, r^{-\alpha}\} r dr d\varphi \end{aligned}$$

$$\begin{aligned} &= 2\pi a_I \lambda \left[\int_0^1 r dr + \int_1^{\infty} r^{-\alpha} r dr \right] \\ &= 2\pi a_I \lambda \left[\frac{1}{2} + \frac{1}{\alpha - 2} \right], \ \alpha > 2. \end{aligned}$$

Now, if the requirement is that the expected interference must be less than the threshold I_{th}, we obtain the following condition:

$$\lambda < \frac{(\alpha - 2) I_{th}}{\alpha \pi a_I}. \tag{4.4}$$

4.1.3.2 CSMA

Next, we assume that each transmitter can transmit packets based on a CSMA protocol and the transmission power is the same for all the transmitters, P_t. By adding the deterministic channel gains between any two nodes in the network to the set of assumptions, there will be an exclusion distance between any two simultaneously active transmitters. This distance is equal to:

$$r_e = d_0 \left(\frac{P_t G_t G_r k}{P_{th}} \right)^{\frac{1}{\alpha}} \tag{4.5}$$

in which G_t is the transmitter antenna gain, G_r is the receiver antenna gain, α is the path loss exponent, P_{th} is the CSMA sensing threshold, and d_0 is the normalizing factor (=1m). k is:

$$k = \left(\frac{c}{4\pi f_c} \right)^2$$

where f_c is the carrier frequency and c is the speed of radio propagation. Next, we uniformly assign a mark to each UAV. A UAV transmits if it has the lowest mark within a disk (B) centered at itself with radius r_e. Therefore, the probability of having a random point transmitting is equal to:

$$\begin{aligned} P_1 &= \sum_{n=1}^{\infty} \frac{1}{n+1} P(|B \bigcap \Phi| = n) \\ &= \sum_{n=1}^{\infty} \frac{1}{n+1} \frac{(\lambda \pi r_e^2)^n e^{-\lambda \pi r_e^2}}{n!} \\ &= \frac{1 - e^{-\lambda \pi r_e^2}}{\lambda \pi r_e^2} \end{aligned}$$

Thus, the new intensity of UAVs transmitting simultaneously can be obtained by using the Campbell's theorem as follows:

$$
\begin{aligned}
A_i &= x_i \quad transmits \\
E[|A \bigcap \Phi|] &= \lambda \int_{\mathbb{R}^2} P(A_i) dx \\
&= \frac{1 - e^{-\lambda \pi r_e^2}}{\lambda \pi r_e^2} \cdot \widetilde{A} \\
\lambda_2 &= \frac{1 - e^{-\lambda \pi r_e^2}}{\pi r_e^2}
\end{aligned}
$$

Following the shot noise theory [59], the mean of aggregate interference from transmitter nodes in a radius b from the receiver node is:

$$
EI = \frac{2k(1 - e^{-\lambda \pi r_e^2}) \left(R_{int}^{2-\alpha} - b^{2-\alpha} \right)}{\alpha - 2}
$$

where R_{int} denotes the distance between the desired receiver and the interferer next to it. If transmission range is represented by R, $R_{int} = r_e - R$. Therefore,

$$
\lambda < \frac{1}{\pi r_e^2} \ln \left(1 - \frac{I_{th}(\alpha - 2) r_e^2}{2k(R_{int}^{2-\alpha} - b^{2-\alpha})} \right) \tag{4.6}
$$

4.1.4 Numerical Results

By combining Equation 4.3 and Equation 4.4, we obtain

$$
\frac{1}{E|S|} \ln \left(\frac{1}{v_{th}} \right) < \lambda < \min \left\{ \frac{1}{\pi d_s^2} \ln \left(\frac{1}{1 - p_s} \right), \frac{(\alpha - 2) I_{th}}{\alpha \pi a_I} \right\}. \tag{4.7}
$$

and by taking Equation 4.3 and Equation 4.6 into account:

$$
\begin{aligned}
&\frac{1}{E|S|} \ln \left(\frac{1}{v_{th}} \right) < \lambda < \\
&\min \left\{ \frac{1}{\pi d_s^2} \ln \left(\frac{1}{1 - p_s} \right), \frac{1}{\pi r_e^2} \ln \left(1 - \frac{I_{th}(\alpha - 2) r_e^2}{2k(R_{int}^{2-\alpha} - b^{2-\alpha})} \right) \right\}
\end{aligned} \tag{4.8}
$$

Equation 4.7 and Equation 4.8 show that fundamental trade-offs exist between transportation, application, and communication measures in UASs. That is, if we want

to increase the coverage, then the safety and interference measures suffer. Therefore, we need to ensure that the minimum transportation, application, and communication performance requirements are satisfied.

To get a better idea about these trade-offs, let's assume that each UAV can on average cover a region as large as 5 hectares, i.e., $E|S| = 50000m^2$ and to avoid collision, we require that the probability that the UAVs get closer than $d_s = 10m$ to each other is as arbitrarily low as p_s, referred to as close-encounter probability. The maximum allowable interference, I_{th} is also fixed to $-40dB$. Moreover, we set α equal to 3 and assume that at any time, half of the UAVs are transmitting, i.e., $a_I = 0.5$. Now for any value of p_s, an upper bound on λ is imposed by Equation 4.7. If we pick this value, again based on Equation 4.7, we come up with a value for v_{th}, i.e., the maximum allowable portion of the area that can be uncovered. It means that smaller values of v_{th} are desired.

Fig. 4.1 shows the coverage-safety-interference tradeoff by plotting v_{th} versus different values of p_s from 0 to 0.02. We want to be as close as possible to the origin, i.e., the ideal case will be when both v_{th} and p_s approach zero. However, we can only achieve values that lie in the indicated achievable region. As p_s decreases, v_{th} goes to 1. In other words, for extremely small close-encounter probability, the coverage is very low. Nevertheless, for reasonable but still very small values of p_s, e.g., 0.01, we can have as large as 80% coverage if there is no interference. In this case, by increasing the value of p_s to .02, v_{th} approaches zero (implying almost 100% coverage). However, the coverage is limited to about 65% if we take the effect of interference into account. In the proposed scenario, choosing $p_s = 0.007$ and $v_{th} = 0.35$ seems to present an efficient trade-off between interference, coverage and probability of close-encounter. Under this tradeoff, the intensity of the UAVs is $2.1 \cdot 10^{-5} \frac{1}{m^2}$.

In addition to the previous assumptions, we assume the transmission power is 1 watt, the transmission range is $200m$, the antenna gains are $23dB$, the carrier

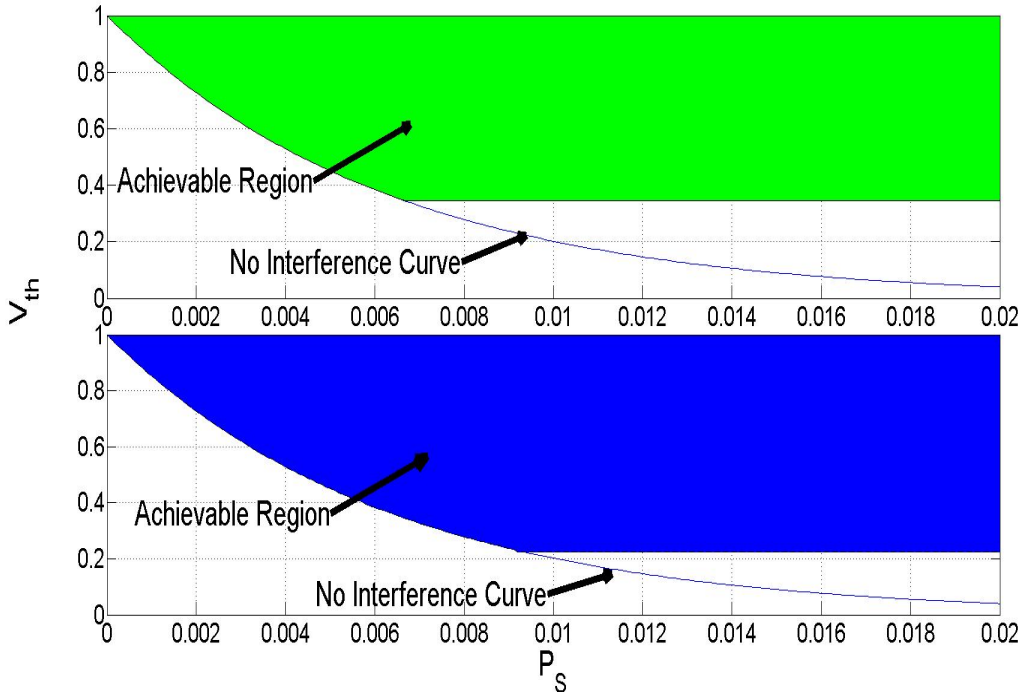

Figure 4.1: The coverage-safety-interference tradeoff. The top figure illustrates the tradeoff when there is no sensing of other UAVs. The bottom one shows the CSMA design.

frequency is $5GHz$ [60] and the CSMA sensing threshold is $-50dBm$ which are all suitable for UAV communication. Fig. 4.1 illustrates that sensing the communication of other UAVs results in a smaller value of v_{th}. $p_s = 0.0092$ and $v_{th} = 0.23$ are achievable under the new design. The new intensity is in the range $[2.94 \cdot 10^{-5}, 2.97 \cdot 10^{-5}]\frac{1}{m^2}$ (obtained by using Inequality 4.8). This shows employing the carrier sensing increases the acceptable intensity of the UAVs.

4.1.5 Connectivity

It has been shown that a 2-D PPP network remains fully connected if the expected number of nearest neighbors of every transmitter grows logarithmically with the coverage area [72]. If we assume the area is infinite, then $\pi R^2 \lambda$ needs to be greater than 10.526 to have a connected component where R represents the transmission range. Therefore,

$$\begin{aligned} &\max\left\{\frac{1}{E|S|}\ln\left(\frac{1}{v_{th}}\right), \frac{10.526}{\pi R^2}\right\} < \lambda < \\ &\min\left\{\frac{1}{\pi d_s^2}\ln\left(\frac{1}{1-p_s}\right), \frac{1}{\pi r_e^2}\ln\left(1-\frac{I_{th}(\alpha-2)r_e^2}{2k(R_{int}^{2-\alpha}-b^{2-\alpha})}\right)\right\} \end{aligned} \tag{4.9}$$

However, the new added part in Equation 4.9 can be removed most of the times. In addition, it does not really demonstrate how the connectivity of the network varies. Hence, we need to assume the scenario with a finite number of UAVs in the network. Each UAS ad hoc network with n UAVs is asymptotically connected with probability one if the UAV is connected to more that 5.1774 $log\ n$ nearest UAV neighbors [73]. Let's assume Z_k denotes the distance of the kth nearest UAV to the transmitter. Since we assume the UAVs are randomly positioned according to Poisson distribution, and each UAV can only transmit signals to receivers in its transmission range, then Z_k has the probability density function:

$$f(z) = \frac{2(\pi R)^k z^{2k-1}}{(k-1)!} e^{-\pi R z^2}$$
$$k = \lfloor 5.1774 \log n \rfloor + 1$$

Therefore, the probability of Z_k being less than R needs to be maximized. This probability equals:

$$P(Z_k < R) = \frac{\gamma(k, \pi\lambda R)}{\Gamma(k)}$$
$$= 1 - \frac{\Gamma(k, \pi\lambda R)}{\Gamma(k)}$$

$\Gamma(k, \pi\lambda R)$, $\gamma(k, \pi\lambda R)$, and $\Gamma(k)$ are upper incomplete gamma function, lower incomplete gamma function, and the ordinary gamma function which are defined as follows:

$$\Gamma(s, x) = \int_x^\infty t^{s-1} e^{-t} dt$$
$$\gamma(s, x) = \int_0^x t^{s-1} e^{-t} dt$$
$$\Gamma(s) = \Gamma(s, x) + \gamma(s, x)$$

Hence, the following fraction can be considered as a connectivity metric:

$$\frac{\int_0^{\pi\lambda R} t^{\lfloor 5.1774 \log n \rfloor} e^{-t} dt}{\int_0^\infty t^{\lfloor 5.1774 \log n \rfloor} e^{-t} dt}$$

It can be seen in Fig. 4.2 (for larger transmission ranges) and Fig. 4.3 (for smaller transmission ranges) that for three obtained intensities $\{2.1 \cdot 10^{-5}, 2.94 \cdot 10^{-5}, 2.97 \cdot 10^{-5}\} \frac{1}{m^2}$ the connectivity increases as the transmission range of UAV increases. More importantly, both Fig. 4.2 and Fig. 4.3 show how a slight increase in the intensity results in a drastic increase in the connectivity. In order to improve the efficiency of packet routing in UAV ad hoc wireless networks, UAVs need to exchange messages to

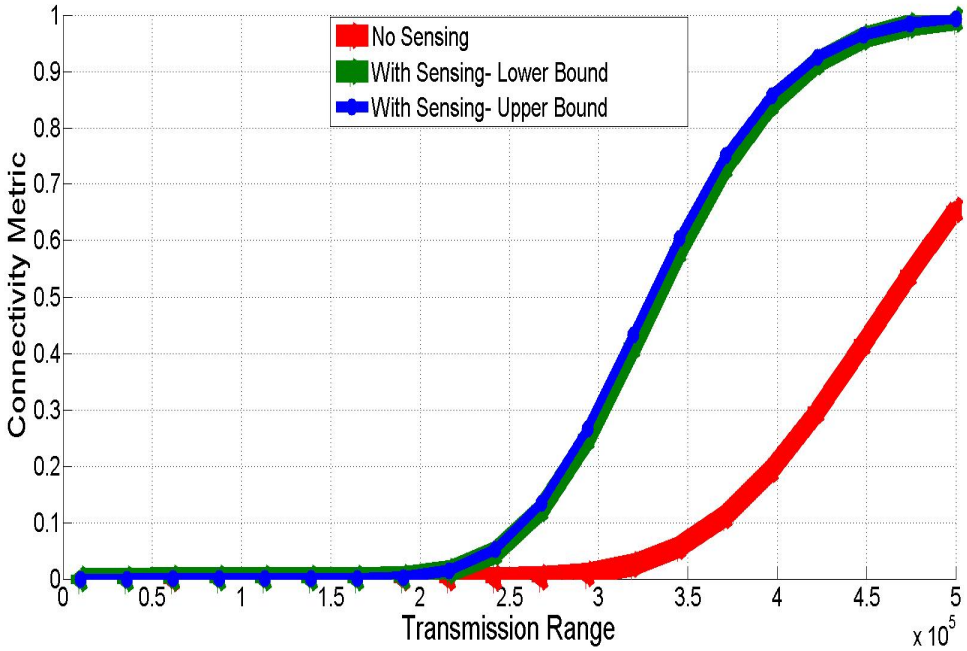

Figure 4.2: The connectivity of the UAV network based on their transmission range for achieved intensities from coverage-safety-interference tradeoff.

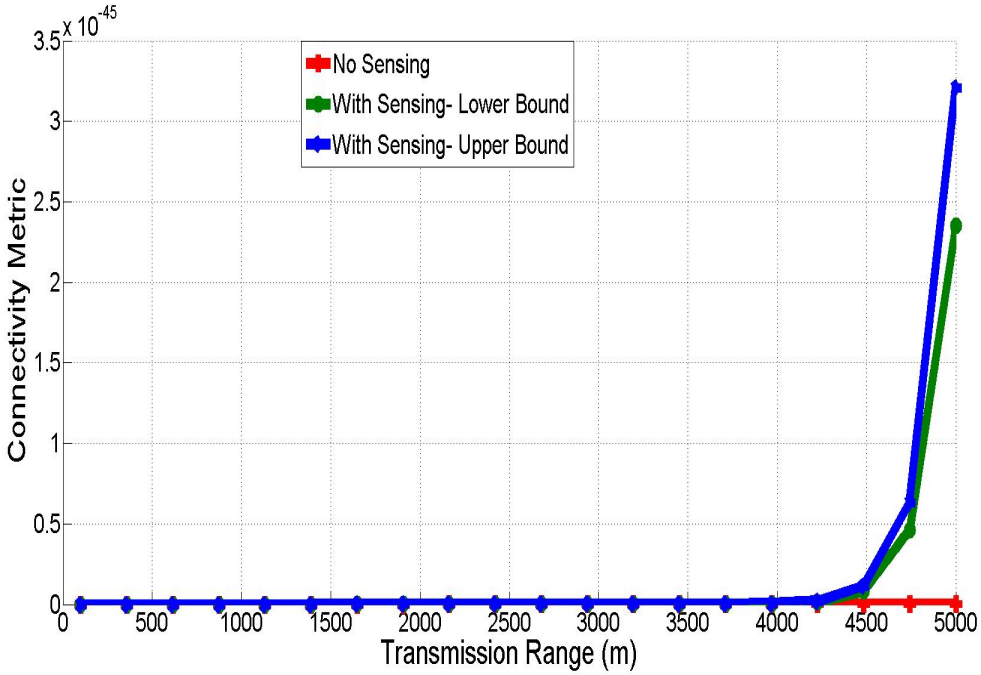

Figure 4.3: The connectivity of the UAV network based on their transmission range for achieved intensities from coverage-safety-interference tradeoff.

make each other aware of the appearances or disappearances of other nodes. Although this process will positively impact the performance of the network, it may lead to packet collisions which may lower the benefits of employing wireless communications.

4.2 Conclusion

In this chapter, we have discussed the tradeoff between coverage, safety, and interference. This combination and the parameters values used in the numerical results section are only suitable for UAVs. This chapter tries to find the suitable geometry (in terms of intensity) needed for those specific applications/requirements. In other words, we bring those tools together to find a geometry which satisfies the specific applications of the UAVs. The interference analysis consists of two parts: with and without carrier sensing. The geometry, carrier frequency, and power sensing threshold are chosen from appropriate values for UAVs based on recent studies. The numerical results show that safety and interference limits the coverage of the network and there is only a relatively small range of intensities which satisfy all three. At last, we studied the connectivity of the network based on a defined metric. Our results illustrate the connectivity of the network varies noticeably even by a very small change in obtained acceptable range of intensities.

CHAPTER 5

CONCLUSION

This dissertation studied the positive effects of customization on VANETs. There are methods available to estimate individual drivers' characteristics from VANETs. In chapter 1, we proposed a regression method to estimate the PRT distribution of a driver which can use all the data in real-time. In addition, we can obtain traffic information (such as distance between vehicles) using vehicular communications. In chapter 2, in order to compute the collision probability, we derived the equations of packet success probability for two extreme cases. Furthermore, we derived the required channel access probabilities for each category of vehicles which are tight approximations of the actual values. If a vehicle has high probability of collision, it needs to transmit more frequently in order to make other vehicles aware of its perilous situation. Finally, we proposed an efficient algorithm to adjust transmission rates of vehicles to safety needs of drivers using the aforementioned data. By employing this algorithm in a network of vehicles, fatalities on highways will be reduced. In chapter 3, the effect of Nakagami-m propagation model on the delivery of safety packets in VANETs was studied. Also, we derived the approximated packet success probability for the scenario which vehicles sense if the channel is idle. In the next chapter, a different approach was employed for a similar type of ad hoc networks. Up to this chapter, our goal was to improve the network performance when the geometry of the network was pre-assumed. In chapter 4, however, we aimed at changing the geometry of the network while a certain level of performance needed to be maintained. Hence, the tradeoff between coverage, safety, and interference was discussed. The numerical

results showed that safety and interference limits the coverage of the network and there was only a relatively small range of intensities which satisfied all three. At last, we studied the connectivity of the network based on a defined metric. Our results illustrated the connectivity of the network varies noticeably even by a very small change in obtained acceptable range of intensities.

APPENDIX

Extension to HCPP-II Model

Although Equation 2.24 leads to a considerable improvement compared to the HCPP model, we can show that adding one condition to this model (we call it MHCPP model) will enhance the system. Let's assume $D_{x_i}(r)$ represents the disk of radius r centered at x_i. The point x_i is retained in Φ_F if

1. $(D_{x_i}(r) \bigcap \Phi) \backslash x_i = \{x_j\}$ such that $m_{x_i} < m_{x_j}$, $\forall x_j \in (D_{x_i}(r) \bigcap \Phi) \backslash x_i$.

2. $(D_{x_i}(r) \bigcap \Phi) \backslash x_i = x_L \bigcup \{x_j\}$ such that $m_{x_i} > m_{x_L}$ and $m_{x_i} < m_{x_j}$, $\forall x_j \in (D_{x_i}(r) \bigcap \Phi) \backslash \{x_i, x_L\}$ given that $S(d) \bigcap \Phi = \{x_k\}$ such that $m_{x_L} > m_{x_k}$, $\exists k \in S(d) \bigcap \Phi$. In other words, the set $S(d) = D_{x_L}(r) \backslash D_{x_i}(r)$ contains at least one point with lower mark than x_L (Fig. 5.1).

where

- Φ represents the parent set of all the nodes.
- m_{x_i} denotes the mark of node x_i which is chosen uniformly from $[0, 1]$.
- $\backslash x_i$ represents the exclusion of the node x_i.

To put it differently, the point $x_i \in \Phi$ is retained in Φ_F:

- if it has the lowest mark in $D_{x_i}(r)$,
- or if it has a second lowest mark in $D_{x_i}(r)$ given that the point x_L with the lowest mark in $D_{x_i}(r)$ does not have the lowest mark in its own disc $D_{x_L}(r)$.

In Fig. 5.1, according to the HCPP-II model, the point A with mark 0.7 is not retained because the point B with mark 0.6 exist in the point A's disk. However, in accordance with the modified HCPP, the point with mark 0.7 is retained since the point with mark 0.5 does not permit the point with mark 0.6 to be retained. Therefore, this model mitigates the node intensity underestimation problem of the traditional HCPP. Deriving the probability of the second part, (P_2), is similar to the derivation of P_1:

$$
\begin{aligned}
P_2 &= \sum_{n=1}^{\infty} \frac{1}{n+1} \frac{N^n e^{-N}}{n!} \sum_{k=1}^{\infty} \frac{k}{n+k+1} \frac{M^k e^{-M}}{k!} \\
&= \frac{M e^{-(N+M)}}{N} \\
&\cdot \left(\sum_{n=1}^{\infty} \frac{N^{n+1}}{(n+1)!} \sum_{k=1}^{\infty} \frac{1}{n+k+1} \frac{(M^{k-1})}{(k-1)!} \right) \\
&= \frac{M e^{-(N+M)}}{N} \\
&\cdot [\frac{e^{N+M}-1}{N+M} + \frac{(M-N)(1-e^M) - NMe^M}{M^2}]
\end{aligned}
$$

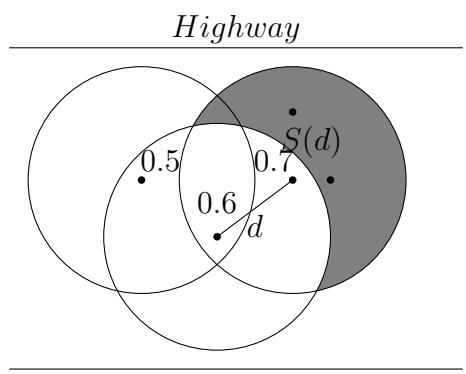

Figure 5.1: Figure explains the modified HCPP. $S(d)$ is the set of points in the gray region.

where k is the number of nodes in $S(d)$, n denotes number of nodes in $D_{x_i}(r)$, N is the expected number of nodes in $D_{x_i}(r)$, and M is the expected number of nodes in $S(d)$. Let's consider two different cases:

1. Single Lane: In a single lane scenario (length L), $N = \lambda_p L$, $M = \lambda_p E(d)$. d denotes the distance between two nodes x_i and x_L. The distribution of d can be assumed to be the Erlang distribution with parameter λ_p.

2. General case: In this case, $N = \lambda_p \pi r^2$ and $M = \lambda_p E_d[S(d)]$ (E_d is the expectation over the random variable d). $S(d)$ is equal to $\pi r^2 - 2r^2 cos^{-1}(\frac{d}{2r}) + d\sqrt{r^2 - d^2/4}$. Also, the distribution of d is given by $f(d) = \frac{2d}{r^2}$, $0 < d < r$ [76].

Therefore, the probability of retaining a random point x_i is:

$$\begin{aligned} P_{tot} &= P_1 + P_2 \\ &= \frac{1 - e^{-N}}{N} + \frac{Me^{-(N+M)}}{N} \\ &\cdot [\frac{e^{N+M} - 1}{N + M} + \frac{(M - N)(1 - e^M) - NMe^M}{M^2}] \end{aligned}$$

The intensity can be obtained as follows:

$$\lambda = P_{tot}/\lambda_p$$

We compare the equal distance model, the HCPP-II model, and the modified HCPP model via MATLAB simulations in order to compare different estimates of the collision probability. We place the vehicles on one lane using the appropriate distributions and the collision probability is calculated when certain number of vehicles are located in $1000m$. Fig. 5.2 illustrates the vehicles' collision probability versus the number of vehicles. If we use the same simulation parameters for the equal-distance scenario, more collisions happen compared to the other two models. Also, Fig. 5.2 shows the

Table 5.1: Simulation Parameters

Distribution	Poisson Equal distance
Velocity	$20\frac{m}{s}$
Deceleration rate	$[-4, -8]\frac{m}{s^2}$
Distance	$1000m$
(Average) distance between vehicles	$25m$
SIR decoding threshold	8 dB
Data rate	6 Mbps
Packet length	250 Bytes

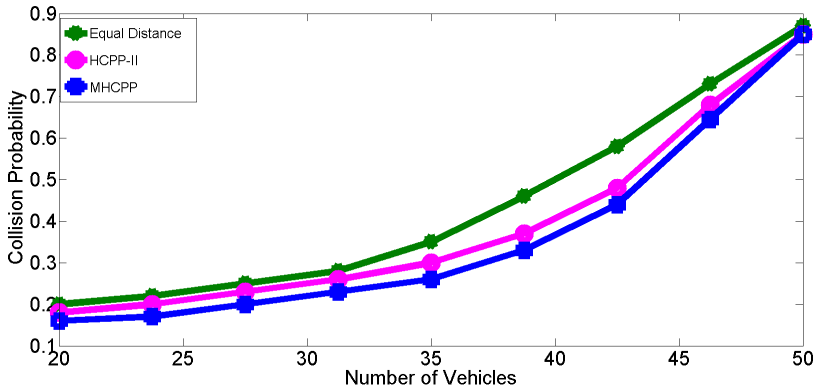

Figure 5.2: Collision probability versus the number of vehicles for three models of vehicles in traffic. All the parameters are given in Table 5.1 except for the number of vehicles which is an independent variable.

achieved improvement based on employing the modified HCPP model rather than employing the HCPP-II model.

BIBLIOGRAPHY

[1] National Highway Traffic Safety Administration, *2013 Motor vehicle crashes: overview,* http://www-nrd.nhtsa.dot.gov/Pubs/812101.pdf, 2013.

[2] United States Department of Transportation, National Highway Traffic Safety Administration, *Early estimate of motor vehicle traffic fatalities in 2011,* Washington D.C., 2012.

[3] *IEEE standard for information technology-telecommunications and information exchange between systems-local and metropolitan area networks-specific requirements part 11: Wireless LAN medium access control (MAC) and physical layer (PHY) specifications amendment 6: Wireless access in vehicular environments*, IEEE Std 802.11p, pp. 1-51, 2010.

[4] A. Rakhshan, H. Pishro-Nik, and E. Ray, *Real-time estimation of the distribution of brake response times for an individual driver for design of active safety systems using VANET*, IEEE Intelligent Vehicle Symposium, pp. 1181-1186, 2014.

[5] S. Al-Sultan, H. Al-Bayatti, and H. Zedan, *Context-aware driver behavior detection system in intelligent transportation systems*, IEEE Transactions on Vehicular Technology, pp. 4264-4275, 2013.

[6] A. Rakhshan, H. Pishro-Nik, M. Nekoui, and D. Fisher, *Tuning collision warning algorithms to individual drivers for design of active safety systems*, Globecom Workshop Vehicular Network Evolution (GC13 WS VNE), pp. 1342-1346, 2013.

[7] W. Jiafu, D. Zhang, S. Zhao, L. Yang, and J. Lloret, *Context-aware vehicular cyber-physical systems with cloud support: architecture, challenges, and solutions*, IEEE Communications Magazine, vol. 52, no. 8, pp. 106-113, 2014.

[8] J.J. Haas, and Y. Hu, *Communication requirements for crash avoidance*, In Proceedings of the seventh ACM international workshop on VehiculAr InterNETworking, pp. 1-10, 2010.

[9] Q. Yi, K. Lu, and N. Moayeri, *CA secure VANET MAC Protocol for DSRC applications*, IEEE GLOBECOM, pp. 1-5, 2008.

[10] B.M. Mughal, A.A. Wagan, and H. Hasbullah, *Efficient congestion control in VANET for safety messaging*, International Symposium on Information Technology (ITSim), vol. 2, pp. 654-659, 2010.

[11] Y. Chang, C. Lee, and J. Copeland, *Goodput enhancement of VANETs in noisy CSMA/CA channels*, IEEE Journal on Selected Areas in Communications, vol. 29, pp. 236249, January 2011.

[12] C. Garcia-Costa, E. Egea-Lopez, J.B. Tomas-Gabarron, J. Garcia-Haro, and Z.J. Haas, *A stochastic model for chain collisions of vehicles equipped with vehicular communications,* IEEE Transactions on Intelligent Transportation Systems, vol. 13, no. 2, pp. 116, 2011.

[13] J. Carbaugh, D. N. Godbole, and R. Sengupta, *Safety and capacity analysis of automated and manual highway systems,* Transportation Research Part C (Emerging Technologies), 1997.

[14] A. May, *Traffic flow fundamentals,* Prentice Hall, pp. 69-70, 1990.

[15] H. Elsawy, E. Hossein, and S. Comorlinga, *Characterizing random CSMA wireless networks: A Stochastic Geometry Approach,* IEEE ICC - Wireless Networks Symposium, pp. 5000-5004, 2012.

[16] F. Farnoud, and S. Valaee, *Reliable broadcast of safety messages in vehicular ad hoc networks*, IEEE INFOCOM Proceedings, pp. 226 234, 2009.

[17] Q. Xu, T. Mak, J. Ko, and R. Sengupta, *Medium access control protocol design for vehicle-vehicle safety messages*, IEEE Transactions on Vehicular Technology, vol. 56, pp. 499518, March 2007.

[18] A. Rakhshan, H. Pishro-Nik, and M. Nekoui, *Driver-based adaptation of Vehicular Ad Hoc Networks for design of active safety systems*, 49th Annual Conference on Information Sciences and Systems (CISS), pp. 1-6, 2015.

[19] N. Deng, W. Zhou, and M. Haenggi, *The Ginibre Point Process as a model for wireless networks with repulsion*, IEEE Transactions on Wireless Communications, vol. 14, pp. 107-121, 2014.

[20] Z. Gong, and M. Haenggi, *The local delay in mobile Poisson networks*, IEEE Transactions on Wireless Communications, vol. 12, pp. 4766-4777, September 2013.

[21] C. Lee, and M. Haenggi, *Interference and outage in Poisson cognitive networks*, IEEE Transactions on Wireless Communications, vol. 11, no. 4, pp. 1392-1401, April 2012.

[22] M.Y. Darus, *Congestion control algorithm in Vanets*, World Appllied Sciences Journal, 2013.

[23] M.Y. Darus, *Dynamic congestion control algorithm for vehicular ad hoc networks*, International Journal of Software Engineering and Its Applications, 2013.

[24] P. Goh, and Y.D. Wong, *Driver perception response time during the signal change interval*, Health Econ Health Policy, 2004.

[25] F.C. Donders, *On the speed of mental processes*, In W. G. Koster (Ed.), Attention and Performance Acta Psychologica, 1869.

[26] J.T. Townsend, and Y.G. Ashby, *The stochastic modeling of elementary psychological processes*, Cambridge: Cambridge University Press, 1983.

[27] R. Ratcliff, *Response time distributions*, Chapter 22 in H. Cooper (Ed.), APA Handbook of Research Methods in Psychology, 2012.

[28] R. Schweickert, D.L. Fisher, and K. Sung, *Descovering cognitive architecture by selectively influencing mental processes*, Advanced Series in Mathematical Psychology, vol. 4, Singapore: World Scientific, 2012.

[29] M. Green, *How long does it take to stop?*, Methodological analysis of driver perception-brake times, Transportation Human Factors, pp. 195-216, 2000.

[30] J.W. Muttart, *Quantifying driver response times based upon research and real life data,* Proceedings of the Third International Driving Symposium on Human Factors in Driver Assessment, Training and Vehicle Design, Rockland, ME: University of Iowa, 2005.

[31] R.D. Luce, *Response times: their role in inferring elementary mental organization*, Oxford: Oxford Univ Press, 1986.

[32] M.S. Chang, and A.J. Santiago, *Timing traffic signal changes based on driver behavior*, Transportation Research Record, pp. 20-30, 1985.

[33] A. Maxwell, and K. Wood, *Review of traffic signals on high speed road. Paper presented at the Europian Transport Conference*, http://www.etcproceedings.org/paper/review-of-traffic-signals-on-high-speed-roads, Accessed 12/2/12, 2012.

[34] R.H. Wortman, and J.S. Matthias, *An evaluation of driver behavior at signalized intersections*, Phoenix: Arizona Department of Transportation, 1983.

[35] X. Zhang, and G.H. Bham, *Estimation of driver reaction time from detailed vehicle trajectory data*, Proceedings of the 18th IASTED International Conference: modeling and simulation, pp. 574-579, 2007.

[36] A. Pollatsek, D. Fisher ,and A.K. Pradhan, *Identifying and remediating failures of selective attention in younger drivers*, Current Directions in Psychological Science, no. 15, pp. 255-259, 2006.

[37] C.E. McCulloch, S.R. Searle, and J.M. Neuhaus, *Generalized, linear, and mixed models*, Hoboken: 2nd ed, Wiley, 2008.

[38] S.R. Searle, G. Casella, and C.E. McCulloch, *Variance components*, New York: Wiley, 1992.

[39] R.J. Koppa, *Human factors*, In Nathan H. Gartner, Carroll J. Messer, and Ajay K. Rathi (Eds.), Revised Monograph on Traffic Flow Theory (Ch.3), http://www.fhwa.dot.gov/publications/, 2005.

[40] J.R. Setti, H. Rakha, and I. El-Shawarby *Analysis of brake perception reaction times on high-speed signalized intersection approaches*, Intelligent Transportation Systems Conference, ITSC, IEEE, 2006.

[41] H. Rakha, I. El-Shawarby, and J.R. Setti, *Characterizing driver behavior on signalized intersection approaches at the onset of a yellow-phase trigger,* IEEE

Transactions on Intelligent Transportation Systems, vol. 8, no. 4, pp. 630-640, 2007.

[42] X. Ma, and I. Andréasson, *Driver reaction delay estimation from real data and its application in gm-type model evaluation,* Journal of the Transportation Research Board, pp. 130-141, 2006.

[43] K.I. Ahmed, *Modeling drivers' acceleration and lane changing behavior*, Ph.D. Dissertation, Massachusetts Institute of Technology, 2006.

[44] N. Ravishanker, and D.K. Dey, *A first course in linear model theory*, Boca Raton: Chapman & Hall/CRC, 2002.

[45] D.V. McGehee, E.N. Mazzae, and G.H.S. Baldwin, *Driver reaction time in crash avoidance research*, Proceedings of the International Ergonomics Association Conference, pp. 320-323, 2000.

[46] A. Rakhshan, E. Ray, and H. Pishro-Nik, *A new approach to customization of collision warning systems to individual drivers*, arXiv preprint arXiv:1408.4111, 2014.

[47] S. Gilani, H. Azmat Shah, A. Qayyum, and H.B. Hasbullah, *Vehicular ad hoc networks for smart cities*, Chapter: MAC Layer Challenges and Proposed Protocols for Vehicular Ad-hoc Networks, Springer, 2015.

[48] H.Q. Nguyen, F. Baccelli, and D. Kofman, *A stochastic geometry analysis of dense IEEE 802.11 networks*, in Proceedings 26th IEEE International Conference on Computer Communications (INFOCOM 07), pp. 1199-1207, 2007.

[49] G. Alfano, M. Garetto, and E. Leonardi, *New insights into the stochastic geometry analysis of dense CSMA networks*, in Proceedings 30th IEEE International Conference on Computer Communications (INFOCOM 11), pp. 2642-2650, 2011.

[50] S. Weber, X. Yang, J.G. Andrews, and G. de vecina, *Transmission capacity of wireless ad hoc networks with outage constraints*, IEEE Transactions on Infromation Theory, vol. 51, no. 12, pp. 4091-4102, 2005.

[51] M.Z. Win, P.C. Pinto, and L.A. Shepp, *A mathematical theory of network interference and its applications*, Proceedings of the IEEE, vol. 97, no. 2, pp. 205-230, 2009.

[52] P. Muhlethaler, and A. Najid, *Throughput optimization of a multihop CSMA moblie ad hoc network*, INRIA, Research Report 4928, 2003.

[53] M. Kaynia, N. Jindal, and G. Oien, *Improving the performance of wireless ad hoc networks through MAC layer design*, IEEE Transactions on Wireless Communications, vol. 10, no. 1, pp. 240-252, 2011.

[54] E.S. Sousa, *Optimum transmission range in a direct-sequence spread spectrum multihop packet radio network*, IEEE Journal Selected Areas in Communications, vol. 8, no. 5, pp. 762-771, 1990.

[55] J.P. Linnartz, *Wireless communication,* http://www.wirelesscommunication.nl/, 2016.

[56] A. Rakhshan, and H. Pishro-Nik, *A new approach to customization of accident warning systems to individual drivers*, IEEE International Multi-Disciplinary Conference on Cognitive Methods in Situation Awareness and Decision Support (CogSIMA), pp. 636-641, 2016.

[57] L. Gupta, R. Jain and G. Vaszkun, *Survey of important issues in UAV communication networks*, IEEE Communications Surveys and Tutorials, vol. 18, no. 02, pp. 1123-1152, November 2015.

[58] M. Haenggi, *Stochastic geometry for wireless networks*, Cambridge University Press, 2013.

[59] J. Venkataraman, M. Haenggi, and O. Collins, *Shot noise models for outage and throughput analyses in Wireless ad hoc networks*, in Proc. IEEE Military Communiation Conference, pp. 1-10, 2006.

[60] D.M. Marshall, R.K. Barnhart, E. Shappee, and M. Most, *Introduction to unmanned aircraft systems*, CRC Press, 2016.

[61] C.C. Murray, and A.G. Chu, *The flying sidekick traveling salesman problem: Optimization of drone-assisted parcel delivery*, Elsevier Transportation Research Part C: Emerging Technologies, vol. 54, pp. 86-109, 2015

[62] F. Furini, C.A. Persiani, A. Carlo, and P. Toth, *The time dependent traveling salesman planning problem in controlled airspac*, Elsevier Transportation Research Part B: Methodological: Emerging Technologies, vol. 90, pp. 38-55, 2016.

[63] O. Bouachir, A. Abrassart, F. Garcia, and N. Larrieu, *A mobility model for UAV ad hoc network*, IEEE International Conference on Unmanned Aircraft Systems (ICUAS), pp. 383-388, 2014.

[64] J. Lee, K. Kim, H. Kim, and H. Kim, *Devising geographic diffusion for drone networks*, Eighth International Conference on Ubiquitous and Future Networks (ICUFN), pp. 76-78, 2016.

[65] J. Lee, K. Kim, H. Kim, and H. Kim, *Civil UAV path planning algorithm for considering connection with cellular data network*, 2012 IEEE 12th International Conference on Computer and Information Technology (CIT), pp. 327-331, 2012

[66] D.W. Matolak, *Unmanned aerial vehicles: Communications challenges and future aerial networking*, 2015 IEEE 12th International Conference on Computing, Networking and Communications (ICNC), pp. 567-572, 2015.

[67] M.J. Marcus, *Spectrum policy challenges of UAV/drones [spectrum policy and regulatory issues]*, IEEE Wireless Communications letter, vol. 21, no. 5, pp. 8-9, 2014.

[68] I. Guvenc, W. Saad, M. Bennis, C. Wietfeld, M. Ding, and L. Pike, *Wireless communications, networking, and positioning with unmanned aerial vehicles [Guest Editorial]*, IEEE Communications Magazine, vol. 54, no. 5, pp. 24-25, 2016.

[69] F. Box, W. Wilson, and L. Globus, *Radio spectrum requirements of control and non-payload communications links for future unmanned aircraft systems*, Air Traffic Control Quarterly, American Institute of Aeronautics and Astronautics, vol. 21, no. 1, pp. 51-78, 2013

[70] F. Jiang, and A.L. Swindlehurst, *Optimization of UAV heading for the ground-to-air uplink*, IEEE Journal on Selected Areas in Communications, vol. 30, no. 5, pp. 993-1005, 2012.

[71] E. Yanmaz, R. Kuschnig, and C. Bettstetter, *Achieving air-ground communications in 802.11 networks with three-dimensional aerial mobility*, In Proceedings of IEEE INFOCOM, pp. 120-124, 2013.

[72] T.K. Philips, S.S. Panwar, and A.N. Tantawi, *Connectivity properties of a packet radio network model*, IEEE Transactions on Information Theory, vol. 35, no. 5, pp. 1044-1047, 1989.

[73] F. Xue, and P.R. Kumar, *The number of neighbors needed for connectivity of wireless networks*, Wireless Networks 10, Kluwer Academic Publishers, pp. 169-181, 2004.

[74] T. Islam, Y. Hu, E. onur, B. Boltjes, and J.F.C.M.de Jongh, *Realistic simulation of IEEE 802.11p channel in mobile vehicle to vehicle communication*, Conference on Microwave Techniques (COMITE), pp. 156-161, April 2013.

[75] M. Killat, F. Schmidt-Eisenlohr, H. Hartenstein, C. Rssel, P. Vortisch, S. Assenmacher, and F. Busch, *Enabling efficient and accurate large-scale simulations of VANETs for vehicular traffic management*, VANET '07 Proceedings of the Fourth ACM International Workshop on Vehicular Ad Hoc Networks, pp. 29-38, 2007.

[76] E.S. Sousa, *Optimum transmission range in a direct-sequence spread spectrum multihop packet radio network*, IEEE Journal Selsected Areas in Communications, vol. 8, no. 5, pp. 762-771, 1990.

[77] A. Rakhshan, and H. Pishro-Nik, *Packet success probability derivation in a vehicular ad hoc network for a highway scenario*, 50th Annual Conference on Information Sciences and Systems (CISS), pp. 210-215, 2016.

[78] A. Rakhshan, and H. Pishro-Nik, *Characterizing successful packet transmission in a vehicular ad hoc network*, IEEE Conference on Computer Communications (INFOCOM), Smart City Workshop, pp. 636-641, 2016.